ENVIRONMENTAL DEGRADATION OF CAST Al-Al$_2$O$_3$ PARTICULATE COMPOSITES

by

GOPINATH. K
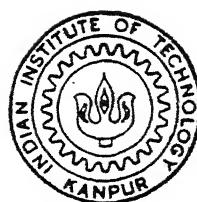
DEPARTMENT OF MATERIALS AND METALLURGICAL ENGINEERING

INDIAN INSTITUTE OF TECHNOLOGY KANPUR

February 1994

ENVIRONMENTAL DEGRADATION OF CAST Al-Al$_2$O$_3$ PARTICULATE COMPOSITES

A Thesis Submitted
in Partial Fulfillment of the Requirements
for the Degree of
MASTER OF TECHNOLOGY

by
GOPINATH. K

to the

DEPARTMENT OF MATERIALS AND METALLURGICAL ENGINEERING
INDIAN INSTITUTE OF TECHNOLOGY , KANPUR
FEBRUARY, 1994

MME-1994-M-GOP-ENV

CERTIFICATE

This is to certify that the work on "Environmental Degradation of Cast Al-Al$_2$O$_3$ Particulate Composites" has been carried out by Mr. Gopinath K under our supervision and that it has not been submitted elsewhere for a degree.

(R. BALASUBRAMANIAM)

ASSIST. PROFESSOR

Deptt. of Materials and
Metallurgical Engg.,

Indian Institute of Technology,

Kanpur 208016

(V.S.R MURTHY)

ASSIST. PROFESSOR

Deptt. of Materials and
Metallurgical Engg.,

Indian Institute of Technology,

Kanpur 208016

February 1994

DEDICATED TO MY PARENTS

ACKNOWLEDGEMENTS

C O N T E N T S

LIST OF TABLES

LIST OF FIGURES

A B S T R A C T

This work is an attempt to study the environmental degradation (corrosion and hydrogen embrittlement) characteristics of as-cast $Al-Al_2O_3$ particulate composites. The composites with 0,2,4 and 8 Weight percentage Al_2O_3 were produced by vortex casting, a new, economic and relatively simple technique of producing composites. Corrosion tests were carried out in 0.1N HCl using electrochemical polarization (Tafel extrapolation) technique. The corrosion rate of the composites increases with increasing reinforcement volume fraction. This has been explained by considering the increase in matrix-reinforcement interfaces with increasing reinforcement additions. The effect of hydrogen on the mechanical properties of the composites was assessed by tensile testing hydrogen pre-charged specimens. Hydrogen charging reduces both the ductilities and ultimate tensile strengths of the composites when compared to the uncharged condition. The degree of hydrogen embrittlement was the least for the $Al-2\%$ Al_2O_3 composite. The degree of hydrogen embrittlement decreased in composites when compared to the base metal. The hydrogen embrittlement behaviour has been explained by considering the reversible and irreversible trap sites in the composites.

CHAPTER 1
INTRODUCTION

1.1 General:

Metals and alloys have the general characteristics of good electrical and thermal conductivity, relatively high strength, high stiffness, ductility and shock resistance. They are easily shaped and joined. They are particularly useful when it comes to structural and load bearing applications [1].* Almost all metals have medium to high density, except for a few light metals like Al, Mg and Be, which is not a big problem for land based engineering systems, but is a big disadvantage as far as aerospace materials are concerned.

Ceramics and glasses have poor electrical and thermal conductivity and high chemical stability. Although they may have high strength, elastic modulus and hardness, their ductility, formability and shock resistance are very poor. Because of their chemical stability they generally are resistant to corrosion in various environments. They also have certain unusual and desirable optical, electrical and thermal properties. They generally are of low density, even though exceptions exist [1].

Polymers, generally are light and have relatively low electrical and thermal conductivity. While thermoplastic polymers are ductile, formable, and shock resistant, thermosetting polymers are not. The most serious problem with polymers is that their mechanical strength and stiffness are low and so in most of the

* References are given at the end of each chapter

applications strength is usually a secondary consideration. Even though they can be easily fabricated and joined they lack thermal stability and are only moderately resistant to environmental degradation [1,2,3].

1.2 Composite Materials:

Composite materials are man-made materials produced when two or more conventional materials are blended intimately to give a combination of properties which cannot be achieved in the original materials. The significance of these materials to the engineer is that their properties can be tailored as per the requirements of the application. They may be selected to give unusual combinations of stiffness, strength, weight, high temperature performance, corrosion resistance, hardness and conductivity [1].

In a composite material, the major phase is termed as 'Matrix'. It is continuous and surrounds the minor, secondary and discretely dispersed phase called 'Reinforcement' [3,4]. The reinforcements basically are of two types- Continuous and Discontinuous. Continuous reinforcements may be in the form of fibers, wires or whiskers whereas discontinous reinforcements can be particulates, platelets, short fibers or whiskers. The volume fraction of these reinforcements is one of the important factors which controls the properties of the composite [3]. It is the presence of these reinforcements that lead to the specific property improvement of the composites.

The first and foremost of the functions of the matrix is to bind the reinforcements togather and hold them intact. It acts as

the medium through which the externally applied stress is transmitted and distributed to the reinforcements in case of load bearing applications [2]. Apart from these important functions they have some secondary functions like protecting the reinforcements from mechanical damage and environmental attack. The potential for reinforcing any given material will depend to some extent on its ability to carry out some or all of the matrix functions, but there are often other considerations. Based on various classes of matrices used composites are classified under three broad categories as

1. Polymer Matrix Composites,

2. Ceramic Matrix Composites and

3. Metal Matri Composites.

1.2.1 Polymer Matrix Composites (PMC):

Inherent polymer characteristics of low density, low electrical and thermal conductivity, extreme mechanical resiliency and transparency combines to provide a good starting point for PMC [5]. While Polypropelene and Nylon 6,6 are commonly used thermoplastics, Polyethersulphone (PES), Polyetheretherketone (PEEK) and polyimides are high temperature thermoplastics commonly used as matrices [3]. Polyester and epoxides are thermosetting plastics which are highly used as matrix material. Commonly used polymeric and ceramic reinforcements in a polymer matrix are in the form of fibers or whiskers and mostly used materials are glass, aramid (Kevlar), carbon, alumina, zirconia, boron and

asbestos [3]. In addition to processing and material variables, temperature and humidity are critical for polymeric matrix composites. Possible deterioration must be known in advance and care is to be taken since both the matrix and reinforcement are affected by these conditions [5]. Another major limitation of PMC is their limited high temperature use. They cannot be used for applications beyond $250^{o}C$ as their thermal stability is very poor.Light weight PMC find extensive applications in aerospace, automobile and sports goods industries.

1.2.2 Ceramic Matrix Composites (CMC):

CMC are among the new class of materials, yet they are being rapidly commercialized [6]. Even though monolithic ceramics such as Si_3N_4, Sialons, ZrO_2 etc., are light and posses high stiffness, good high temperature strength, thermal stability and resistance to oxidative environments, they are yet to be fully exploited as structural components due primarily to their limited fracture toughness, poor structural reliability, and/or reproducibility [7]. They also exhibit a wide variation in strength properties due to variation in flaw sizes which are very difficult to control during the processing of ceramics. One way of improving the reliability of ceramics is by opting to CMC. SiC and Si_3N_4 based ceramic materials offer best potential for high temperature structural component both as matrix and reinforcement. Reinforcements incorporated into CMC are basically aimed at improving the toughness of ceramics. So, a weak interface is preferred in the case of CMC between the matrix and fiber as they

can deflect an incoming crack along the interface thereby increasing the crack path length and hence fracture toughness [8]. High strength refractory fibers of Carbon, SiC, Al_2O_3 and Si_3N_4 or whiskers of SiC and Si_3N_4 are commonly used as reinforcements in glass or glass ceramic matrix composites or conventional monolithic ceramics like SiC, Si_3N_4, Al_2O_3 etc., Among particulates TiC, SiC, BN, and ZrO_2 for transformation toughening are the commonly used particulates and they are used in matrices of Al_2O_3, Si_3N_4, Carbon or glass ceramics. These ceramic matrix composites are under extensive study as they are potential materials for automotive and aerospace application because of their increasing reliability coupled with light weight, good mechanical properties and oxidation resistance. The processing of ceramic matrix composites is quiet complex because of the inherent problems associated with thermal expansion mismatch, dispersoid clustering and low interdiffusivity between the matrix and the reinforcement [9].

1.2.3 Metal Matrix Composites (MMC):

Increasing requirements from industrial and military designs for strong, rigid, light and heat resistant materials lead to the development of MMC [5]. They are materials with potential for structural and thermal management applications. They are capable of providing higher temperature operating limits than their base metal counterparts and they can be tailored to give improved strength and modulus, thermal conductivity, thermal shock resistance, abrasion and creep resistance and dimensional

stability. Initial development was in the field of fiber reinforced MMC for usage in aerospace applications. The expansion into non-aerospace and non-military fields came slowly as the cost of MMC started decreasing because of the development of low cost reinforcements- both continuous and discontinuous [10].

In a MMC, normally, the matrix phase is a metal or alloy and the reinforcements are either ceramic or metallic. The presence of a metal as a matrix imparts metallic nature to the composite in terms of thermal and electrical conductivity, manufacturing processes and interaction with the environment [11]. Generally, matrices are tough, ductile and resistant to environmental attack and reinforcements are stiff, strong, light, thermally stable and compatible with the matrix. Commonly used matrices are alloys of Al, Cu, Ti, Mg, Zn, Ni and Fe [12]. MMC contain reinforcements from 0 to 60 volume%, either in continuous or discontinuous form. Continuous reinforcements like fibers and filaments of Carbon, SiC, Boron or Al_2O_3 and discontinuous reinforcements like particulates or pletelets of SiC, Al_2O_3, or TiB_2 are commonly used. Interface between the matrix and the reinforcement is of paramount concern for composite mechanical properties, since the load is transferred from the matrix to the reinforcement via interface [13]. To maximize interfacial bond strength it is necessary to improve wetting between the matrix and the reinforcement, control chemical interactions and minimize oxide formation [14].

Recent research in discontinuously reinforced MMC has shown

that they are also amenable to common metal forming operations, including extrusion, forging and rolling [10]. This led to the usage of discontinuously reinforced MMC in a variety of applications like automobile engine components, pistons and connecting rods where stiffness to strength ratio is important. Their high temperature performance is better than that of matrix alloys and are more reliable high temperature material systems than CMC [12]. However, they too have certain disadvantages like low fracture strain and fracture toughness and are also prone to thermal fatigue.

Among all the MMC, Al alloy composites has been studied extensively [10]. Its useful mechanical properties coupled with light weight and resistance to environmental attack and ease of fabrication has made it a quiet successful composite. Discontinuously reinforced SiC/Al MMC are developed by aircraft industry for use as airplane skins, intercostal ribs and such other applications. Graphite/Al MMC are being used as inexpensive anti-friction material. Particulate reinforced MMC are candidate materials for moving parts of automotive engines, such as pistons, connecting rods, piston pins and various components in cylinder head and valve train because of their wear resistance [10]. Al alloys (of 5000 series and 6061Al) reinforced with graphite fibers, which has excellent strength and modulus, has been considered for marine and high-technology naval applications. Utilization of MMC in marine environments requires adequate corrosion resistance [15,16]. Thus it becomes essential to study

the effect of environment on the properties of these materials. An attempt has been made in this direction through this work.

References:

1.   D.R.Askeland,"The Science and Engineering of Materials", p1, Brooks/Cole Engineering Division, Montery (1984).

2.   B.Harris,"Engineering Composite Materials", p6, The Institute of Metals Publications, Brookfield (1986).

3.   G.Weidmann, P.Lewis and N.Reid eds.,"Structural Materials-Materials in action series", The Open University, Keynes (1990).

4.   W.D.Callister,"Materials Science and Engineering - An Introduction", p389, John Wiley and Sons, New York (1985).

5.   E.Scala, "Composite Materials for Combined Function", Hayden book Co., New Jersey (1973).

6.   "Advances in High Tech Materials.Data File-III", p21 Technical Insights Inc., New Jersey (1987)

7.   D.L.M.Danels, T.T.Serafini and J.A.Di Carlo, Polymer,metal and ceramic matrix for advanced aircraft engine applications, in "Advanced Composites-Conference Proceedings", p263, The ASM,Metals Park (1985).

8.   W.Donald and P.W.McMillan, Review:Ceramic-Matrix Composites, J.Mater.Sci., 11, 949 (1976).

9.   B.Cales, Ceramic Matrix Composites, ed.,R.F.Riley in "2nd European Symposium on Engineering Ceramics", p171, Elsevier Applied Science, New York (1989).

10. M.Taya and R.J.Arsenault, "Metal Matrix Composites-Thermo mechanical Behavior", p2, Pergamon Press, New York (1989).

11. Metal Matrix Composites, in "Metals Handbook", p903, 10th ed,

Vol.2, ASM Publications, Metals Park (1990).

12. B.Terry and G.Jones, "Metal Matrix Composites – Current Developments and Future Trends in Industrial Research and Applications", p5, Elsevier Advanced Technology, Oxford, (1990)

13. A.K.Ghosh, Processing of Metal Matrix Composites, ed. R.Trivedi, J.A.Sekhar and J.Mazumdar in "Principles of Solidification and Materials Processing", p585, Oxford and IBH Publication Co., New Delhi (1989).

14. I.A.Ibrahim, F.A.Mohammed and E.J.Lavernia, Particulate reinforced metal matrix composites- a review, J.Mater.Sci., 26, 1137 (1991).

15. D.M.Aylor and P.J.Moran, Effect of Reinforcement on the Pitting Behavior of Aluminium-Base Metal Matrix Composites, J.Electrochem.Soc., 132, 1277 (1985).

16. M.Saxena, B.K.Prasad and T.K.Dan, Corrosion Characteristics of Aluminium Alloy Graphite Composite in Various Environments, J.Mater.Sci., 27, 4805 (1992).

CHAPTER 2

LITERATURE REVIEW

2.1 Discontinuously reinforced Metal Matrix Composites (MMC):

Early studies on MMC were focused on development of continuous fiber reinforced composites. Despite the encouraging initial results, extensive industrial applications has been hindered by the high manufacturing costs of the continuous reinforcing fibers. Consequently utilization of these materials became restricted for military and other highly specialized applications. On the other hand availability of cheap, discontinuous reinforcements, successful development of manufacturing processes to produce discontinuously reinforced MMC and their easy workability has attracted considerable attention of the researchers towards discontinuously reinforced MMC. Whiskers and particulates are commonly used discontinuous reinforcements. These composites can offer isotropic properties with substantial improvement in strength and stiffness over the matrix for applications, especially in automotive components, which do not require extreme loading or thermal conditions [1]. Although reinforced MMC are better than particulate reinforced ones from strength and thermal stability point of view, the relatively high cost of whiskers and faulty internal structure of whiskers has made particulate reinforced composites industrially viable and attractive . In this context, the low density and reasonably high thermal conductivity of Al has made it the most commercially exploited matrix material. SiC, Graphite, and Al_2O_3 are are the

most commonly used particulate reinforcements in Al matrix composites.

2.2 Matrix-Reinforcement Interface:

The interface between the metallic matrix and the ceramic reinforcement is of extreme importance since the characteristics of this region decide the effectiveness of load transfer and crack growth resistance of MMC on elastic and plastic deformation [1,2]. Ceramic-Metal interfaces of high integrity are required for several areas of advanced technology but are difficult to produce because of the markedly differing lattice bonding characteristics of ceramics and metals [3]. While bonding electrons in metals are delocalized, the movement of electrons in ceramics is restricted by the ionicity or covalency of their lattices. Thus the nature of the lattice bonding changes abruptly at ceramic-metal interfaces. In order to maximize the interfacial bond strength in MMC, it is necessary to promote wetting and control interactions between the matrix and the reinforcement. Wetting is difficult to achieve in molten metal-ceramic systems as a result of high surface tension commonly associated with molten metals (of the order of 1000 mJ/m^2 [1]). Wetting angle or Contact angle, θ is a measure of wettability between a solid and liquid (Figure 1). According to Young's equation,

$$\gamma_{sg} = \gamma_{lg} \cos\theta + \gamma_{sl}$$

where γ_{sl}, γ_{sg}, γ_{lg} are the interfacial energies between solid and liquid, solid and gas and liquid and gas phases respectively. Wetting is achieved when $\theta < 90^o$ (i.e., when $\gamma_{sg} > \gamma_{sl}$).
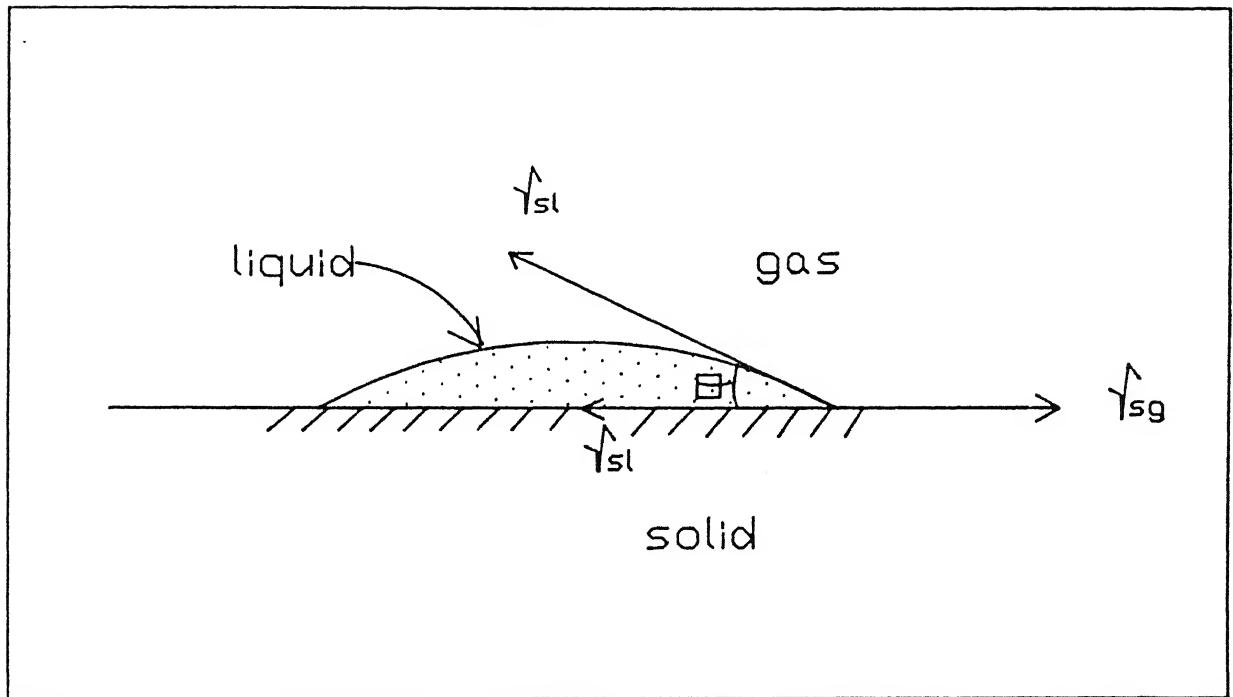
'igure 1.   Schematic diagram showing contact angle formed   between   solid,
liquid and gas phases.

Al is a reactive metal and is therefore expected to react with a vast majority of reinforcements. However the reaction rate is very slow because of the presence of a protective alumina layer which persists through processing or is formed *in-situ* [4]. The presence of this oxide film leads to high contact angle values [4,5]. In practice wettability can be improved by

(a). applying metallic coatings to the ceramic particulates so that the nature of interface changes from metal-ceramic to metal-metal (for example Ni coated graphite for Al matrix [6])

(b).adding reactive elements such as Li, Mg, Ca, Ti, Zr or P to the matrix. It will reduce the surface tension of the melt, reduce γ_{sl} of the melt and induce chemical reaction at the interface. Addition of 3% Mg to Al reduces the surface tension of Al from 0.76 to 0.62 J/m^2 at 933K. Al_2O_3 readily reacts with many divalent transition metal oxides to form aluminates. For example, with Mg it forms $MgAl_2O_4$ spinel. These mineral spinels or similar oxides promote interfacial bonding since they form strong bonds with both the metal and ceramic [7-12]. Similarly, SiC reacts with Al to form Al_4C_3 by the reaction [13]

$$4\ Al\ +\ 3\ SiC\ =\ Al_4C_3\ +\ 3\ Si$$
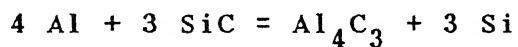
The Si formed by the reaction dissolves in the matrix. However this reaction is normally very slow and takes place at temperatures greater than 900K. The problem with this reaction is that it degrades the reinforcement and also the reaction product is generally rough and leads to stress localization.

(c).heat treating ceramic particulates. This results in desorption of adsorbed gases from ceramic surfaces on heating. On TiO_2 and ZrO_2 particles, chemisorbed water existing in the form of surface hydroxyls further physisorb water molecules through hydrogen bonding. Heat treating the ceramic particulates before incorporating them into the melt drives off these surface hydroxyls and other adsorbed gases and improves wettability [14].

2.3 Processing of MMC:

The processing methods for producing MMC can be widely classified in to three categories [1] as

1. Liquid phase processes,

2. Solid state processes and

3. Two phase (Solid-Liquid) processes

2.3.1 Liquid phase processes:

In liquid phase processing, ceramic particulates are incorporated into a molten metallic matrix using various techniques and is followed by casting . Few of the approaches to introduce ceramic particulates into an alloy melt include (a) Injection of powders entrained in an inert carrier gas into the melt (b) Addition of particulates into the melt via a vortex introduced by mechanical agitation (Vortex casting) (c)Addition of small briquets in to the melt followed by stirring. These processes generally favor intimate interfacial contact and hence a stronger bonding between matrix and reinforcement. However certain inherent disadvantages like the formation of brittle interfacial reaction layer, agglomeration of particles, particle fracturing

during mechanical agitation and introduction of porosity. Squeeze casting is another method wherein pressure is imposed on a solidifying composite system using a hydraulically activated ram. This results in a fine microstructure and low porosity level in the castings. Application of pressure to molten metal infiltrating through a preform called, squeeze infiltration, is also used to process MMC. Melt oxidation processing (called Lanxide processing) is another method to process MMC. In this process a molten alloy infiltrating a ceramic preform undergoes an oxidation reaction with a gas phase (commonly air). This oxidation of molten alloy in the interstices of the preform results in a matrix composed of a mixture of oxidation reaction products and unreacted metal alloy [1].

2.3.2 Solid state processes:

The most common solid state processing technique is powder blending and compaction (i.e., Powder metallurgy route). After blending the reinforcements with matrix powder, cold isostatic pressing produces a green compact. The green compact is then degassed and final compaction is done by extrusion, forging, rolling or some other hot working method [1,3].

2.3.3 Two phase processes:

The most important among the two phase processes is Rhoecasting (also called as Slurry casting). In this method the liquid alloy at a temperature 30-50K above liquidus is vigorously agitated and allowed to slowly cool to the semisolid range. The continued agitation breaks up the solidifying dendrites into fine

spheroidal particles and prevents a rise in viscosity of the slurry. While the stirring continues, reinforcement particles or whiskers are added to the semisolid slurry. This slurry is directly cast into billets. Alternatively, the semisolid composite mixture can be reheated to just above liquidus (to reduce the viscosity in order to allow the mixture to flow into the molds) and die-cast into net-shape components. This process is termed as Compocasting [2]. Osprey deposition process is a two phase process wherein the reinforcement particles are introduced in to the stream of molten alloy which will be atomized by jets of inert gas and collected on a substrate as a billet. It combines the blending and consolidation steps of the powder metallurgy route [1,3].

2.4 Mechanical Properties of Particulate Composites:

The parameters controlling the mechanical properties of particulate reinforced composites are not understood in detail [15]. However certain important factors have become apparent. A schematic stress-strain diagram for a composite is shown in Figure 2. The property which is least sensitive to microstructural features is the modulus. However, the modulus of a composite is a function of volume fraction and modulus of reinforcement. The yield and ultimate strength of composites are sensitive to a variety of factors. Addition of particulate reinforcement provides very little increase in proportionality limit, but produces a large increase in yield stress. Composites have a much larger work hardening rate at low strains (Figure 3) and this is the main strengthening contribution from the particulates. The work
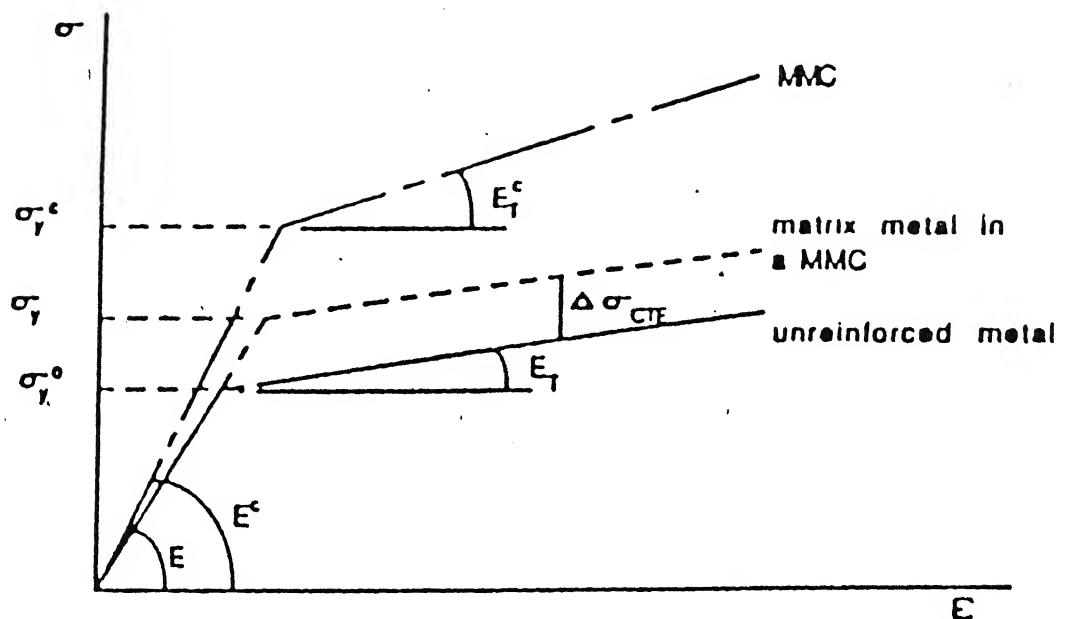
Figure 2. Schematic Stress-Strain diagram for a composite materia
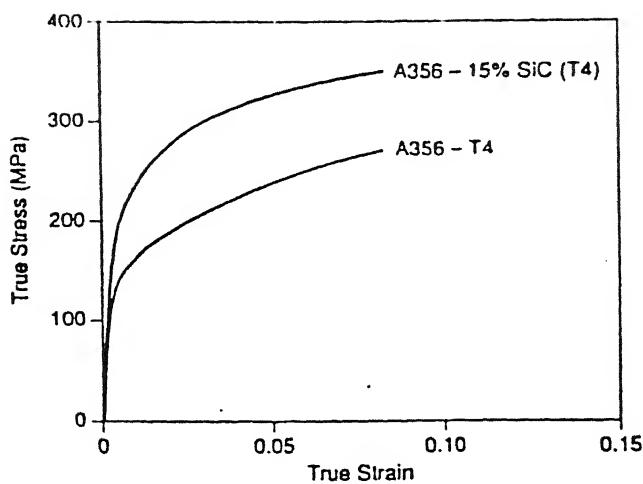
Figure 3. Stress-Strain curves of A356 and A356- 15 Vol% SiC composi[...]
showing high work hardening rate for composites.
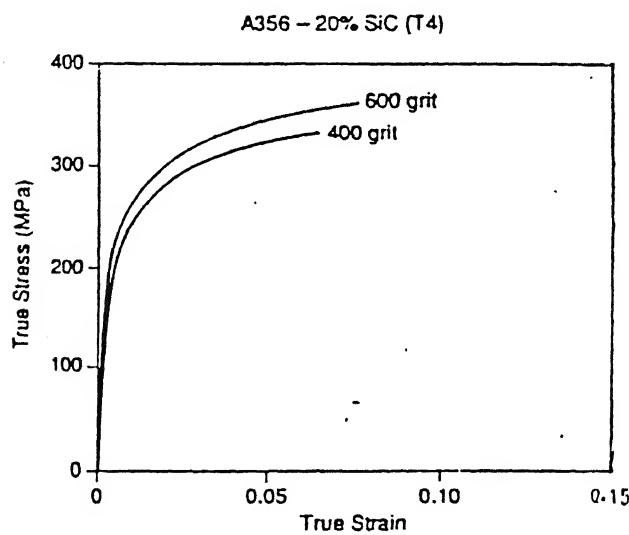
Figure 4. Dependence of work hardening rate on particle size.

hardening rate at low strains is dependent on particle size as shown in Figure 4 [15]

2.4.1 Strengthening mechanisms:

The strength of a crystalline solid is determined by the stress required to either generate or move dislocations across the lattice. The later is a more important factor for two-phase systems. In particulate reinforced MMC dislocation motion is controlled by dislocation-dislocation or dislocation-particle interactions. Thermal stresses and misfit strains are generated at the interfaces of the particle and the matrix due to the difference in coefficient of thermal expansion (CTE) between the matrix and the reinforcement. These misfit strains are sufficient to generate dislocations at the reinforcement-matrix interface. In Al-SiC MMC, the Al matrix has a CTE ten times that of SiC and hence, a misfit strain of 1% is developed at the circumference of SiC particulates [1]. This results in a high dislocation density $(1.8 \times 10^{13}/m^2)$ at the interface. These dislocations form a dislocation induced substructure at the interface. This has been confirmed by high voltage electron microscopic studies [16]. When matrix metal in a particulate MMC deforms plastically, internal stresses arise as a result of the particulates which deform elastically, resisting the plastic flow of the matrix. This internal stress is referred to as `back stress'. The presence of these back stresses increase the flow stress in particulate MMC [18]. Another factor responsible foe the increase in strength of composites is the reduction in sub grain size [19] with

incorporation of particulates. Residual stresses also contribute to strengthening of a particulate MMC. Therefore the predicted yield strength ($\Delta\sigma_{Y,PREDICTED}$) is given by [19]

$$\Delta\sigma_{Y,PREDICTED} = \Delta\sigma_{CTE} + \Delta\sigma_{SG} - \Delta\sigma_{RES}$$

Where $\Delta\sigma_{CTE}$ is the increase in yield stress due to CTE mismatch, $\Delta\sigma_{SG}$ is the contribution towards increase in yield stress because of reduced sub grain size and $\Delta\sigma_{RES}$ is the predicted average residual tensile stress.

The presence of dislocations in the matrix also accelerates the aging kinetics of the matrix alloy if the matrix is precipitation hardenable [19]. Precipitation is facilitated in these cases as the interfacial dislocations act as nuclei for precipitates. All the above said factors result in increasing the strength of a MMC by altering the nature of the matrix. It is also reflected in the increasing hardness values with increasing reinforcement fraction [21].

Porosity is an important factor which influences both the high temperature and room temperature mechanical properties the composites, especially cast MMC. Micropores are an inherent part composites and cannot be avoided as has been widely reported by several researchers. Variation of porosity in a cast MMC with increasing Al_2O_3 content is shown in Figure 5 [20-25]. Moreover, particle distribution is not uniform in cast MMC and so deformation response of particle clustered regions will be different from the rest of the composite. The elastic particles constrain the deformation of the adjacent matrix and this results
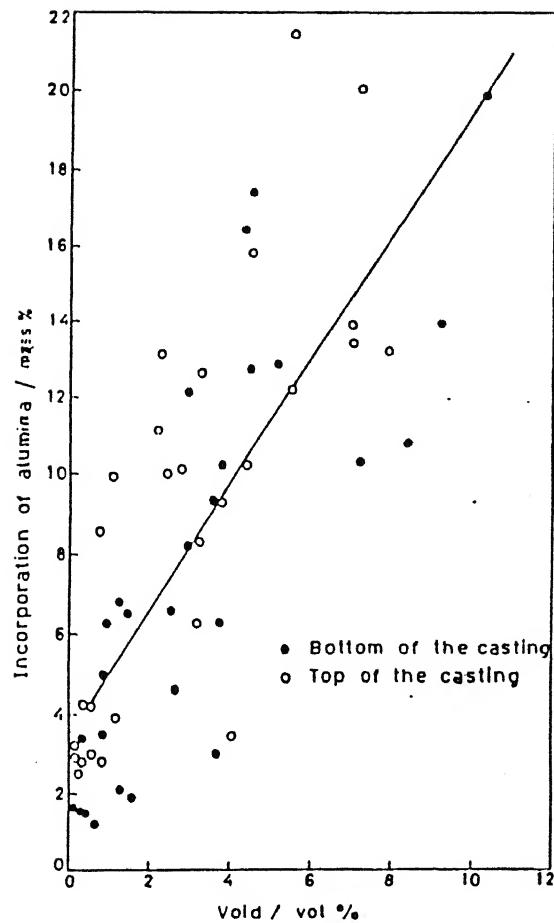
Figure 5. Variation of porosity in a cast $Al-Al_2O_3$ composite

in complex triaxial stresses in the matrix within clusters. Triaxial stresses are important because they enhance both void nucleation and void growth mechanisms.

2.5 Hydrogen Embrittlement of Metals and Alloys:

Hydrogen with only one proton in the nucleus migrates readily through the crystal structure of most metals and alloys due to its small size. Hydrogen damage includes a number of detrimental effects on metallurgical and mechanical properties, resulting from the hydrogen dissolved in the crystal lattice. FCC metals are more resistant to hydrogen damage than BCC metals because of their inherent high ductility and lower diffusivity for hydrogen, but can become susceptible if highly cold worked. Hydrogen dissolved in the matrix drastically affects mechanical strength and ductility. In many FCC alloys, the effect of hydrogen is primarily to decrease the plastic strain to failure. Many modern Al alloys have shown significant susceptibility to hydrogen damage and have been subject of extensive study, although pure Al has been shown to be comparatively insensitive to gaseous hydrogen environments [26,27].

Hydrogen can form on a metal surface from various sources like cathodic reduction of hydrogen or water according to the following reactions:

$$2\ H^+ + 2e^- \longrightarrow H_2 \qquad\qquad\qquad (1)$$

$$2\ H_2O + 2e^- \longrightarrow H_2 + 2\ OH^- \qquad\qquad (2)$$
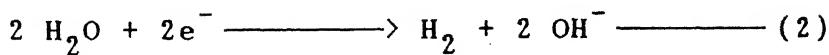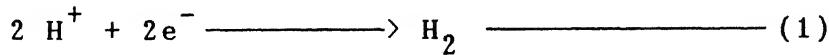
This hydrogen liberation reaction is composed of several steps like

(i) diffusion of H^+ to the surface

(ii) adsorption of H^+ on the surface

(iii) reduction of H^+ to H (i.e., $H^+ + e^- \longrightarrow H$)

(iv) recombination of atomic hydrogen to molecular hydrogen

(v) formation of hydrogen bubbles and their outward diffusion. These cathodic reactions may occur during corrosion on environmental exposure, cathodic protection, pickling and other cleaning operations. Hydrogen enters the lattice as nascent or atomic hydrogen which is an intermediate in the formation of molecular hydrogen on the surface by reaction (1) or (2). Processes involving cathodic polarization, such as cathodic protection and electroplating accelerate hydrogen formation by (1) or (2). `Hydrogen recombination poisons' retard the formation of molecular hydrogen ( step (iv) above ) and increase the residence time of nascent hydrogen on the surface. This enhances hydrogen entry and can sufficiently increase hydrogen damage. Commonly known `poisons' include phosphorus, arsenic, antimony, sulfur, selenium, tellurium and cyanide ions [28].

A generally recognized common feature of all theories and experimental results of hydrogen embrittlement is that some critical concentration of hydrogen must be reached at potential crack sites for failure to initiate [29,30]. Hydrogen diffusing through the lattice accumulates at metallurgical inhomogeneities called `traps'. Pressouyre and Bernstein classified the possible

hydrogen hydrogen in a material into two wide classes as reversible traps and irreversible traps. Reversible traps exchange hydrogen with stronger traps thereby acting as hydrogen sources. Irreversible traps act as sinks and hydrogen get trapped to them permanently. Consequently the interaction energy between a reversible trap and hydrogen is lower compared to the interaction energy between an irreversible trap and hydrogen. Coherent phase interfaces, dislocations, low angle boundaries, microvoids and solute atoms with affinity for hydrogen are reversible hydrogen traps whereas incoherent phase interfaces, high angle grain boundaries, pre existing or propagating microcracks are irreversible hydrogen traps [31,32]. Some of these traps will be potential flaws,i.e.,they may nucleate cracks; whether or not a crack will start depends on the trapping capacity of the trap, on its critical concentration value and on the quantity of hydrogen that will reach the trap site during the test. If the quantity goes over the critical concentration, a crack will be nucleated. Irreversible traps prevent hydrogen from reaching potential flaws in sufficient quantities thereby acting as innocuous sinks whereas reversible traps can help potential flaws in gaining large amount of hydrogen (i.e.,Reversible traps can act both as source and sink).

2.5.1 Mechanisms of hydrogen embrittlement:

Various mechanisms has been proposed to account for the role of hydrogen in reducing the ductility and/or the fracture strength of materials. A few prominent among them are

(1) High pressure bubble formation

(2) Surface adsorption effects

(3) Plastic deformation effects

(4) Decohesion and

(5) Hydride precipitation

A single mechanism has not been able to explain all hydrogen embrittlement phenomena fully. In some metals embrittlement is due to the formation of high pressure hydrogen bubbles. The sum of externally applied stress and internal pressure leads to the propagation of cracks from these high pressure bubbles. However, this theory cannot explain the change in fracture mode from ductile to brittle by the presence of high pressure bubbles [33].

The surface adsorption mechanism of hydrogen embrittlement [35] states that hydrogen reduces the effective surface energy (γ) as a result of adsorption on the surface produced as the crack propagates and this consequently reduces the fracture stress. Objection raised is that effective surface energy (γ), which is a sum of thermodynamic surface energy (γ_s) and energy of plastic deformation (γ_p), will not change to any considerable extent because of the changes in γ_s, which as a whole is a much smaller quantity when compared with γ_p. So, fracture stress should not be markedly affected.

Hydrogen related fracture mechanisms based on changes in plastic properties too are contradicting in nature. Stroh [35] suggested that hydrogen embrittlement of steels could be due to solution strengthening at crack tips because of dissolved

hydrogen, leading to decrease in plastic accommodation and blunting, thus decreasing fracture toughness. This has been contradicted in Beachem's view [36] that stress induced hydrogen segregation at the crack tip aids plastic deformation, which ultimately leads to failure. Although Birnbaum and co-workers have shown by *in-situ* TEM that hydrogen enhances plasticity at the crack tips, a detailed mechanism relating hydrogen enhanced local plasticity and fracture has not been put forward.

Decohesion mechanism states that presence of hydrogen as solute decreases the atomic bond strength and when local stress exceeds the atomic bond strength or cohesive stress, σ_c fracture occurs. However, variation of σ_c with hydrogen concentration is not established.

In some metallic systems brittle hydrides are known to form and have been shown to nucleate cracks [38] but the propagation mechanism in the absence of hydrides is not known. Stress induced hydride formation would also lead to embrittlement in systems like Nb-H, Ti-H and Zr-H where the hydrides are stable at room temperature and atmospheric pressure.

2.6 Hydrogen Embrittlement of Particulate MMC:

Alloying and metallurgical treatments to modify micro structural features modifies hydrogen trapping tendency also because most metallurgical features like high and low angle boundaries, dislocations and interfaces are basically hydrogen traps. This offers a promising avenue to the development of materials with maximum resistance to hydrogen damage. Consistent

with the hydrogen trapping theories, deep or irreversible trapping should reduce the population of hydrogen at crack tips. The hydrogen trapping characteristics of the Fe-Ti-C alloys with large incoherent TiC carbide particles prove this point [32]. Experiments conducted on ODS materials like Pd-Al_2O_3, Pd-MgO, Pd-ZnO and Pd-ZrO_2 alloys [39] (prepared by internal oxidation) to study the influence of oxide-metal interface on hydrogen trapping showed strong trapping of hydrogen in all the alloys. It was concluded that internal oxidation left excess oxygen at the interfaces aiding the formation of O-H bonds and making them strong irreversible traps of hydrogen. An increase in alumina content of alumina dispersed copper alloys has been reported to have beneficial effect on the ductility of these alloys after hydrogen charging. This was attributed to the higher number of irreversible trapping sites (metal-oxide interfaces) in the material containing higher alumina compared to lower alumina containing ODS copper alloys [40]. Interestingly, a reduction in the dislocation density (i.e.,reversible traps) reduced the ductility losses on hydrogen charging [40]. Hydrogen embrittlement characteristics of particulate reinforced MMC having incoherent interfaces has not been reported in literature.

2.7 Corrosion of MMC:

Interest in implementation of MMC in marine applications is rapidly expanding due to the materials' higher strength and modulus than can be attained by conventional alloying. Although incorporation of a second reinforcing phase in to a matrix

material can enhance the physical and mechanical properties of the material, it can also significantly change the corrosion behavior. To date, composites considered for marine applications are typically aluminium based, specifically 5000 series or 6061 Al with reinforcements of SiC and graphite [41,42]. Al, which has a film covering its surface and is passive in aqueous electrolytes, is subjected to intense localized corrosion in the presence of chloride ions. This fact and the nature of environment in naval and marine applications resulted in corrosion studies that were conducted on the composites in simulated sea water and acid media containing chloride ions. These studies revealed that corrosion damage of composites exposed to sea water and acid medium were mainly localized in contrast to uniform corrosion observed for the base alloy and also the composites were found to corrode faster than the base alloy even though the attack was mainly localized [43-47]. The oxide film on the surface of Al MMC is not continuous due to the presence of reinforcements which lead to the breakdown of the film at the matrix-reinforcement interfaces. Therefore corrosion initiates easily at these discontinuities and so composites are more prone to corrosion than the unreinforced matrix [45-47]. In Al-graphite composites, apart from the attack at the interfaces due to film breakdown, the cathodic nature of graphite to the Al matrix results in the formation of a galvanic coupling the presence of an electrolyte [41,42,48]. Studies in Al-mica system also indicate similar results [46].

2.7.1 Corrosion techniques:

2.7.1.1 Weight loss method:

Corrosion damage is most commonly assessed by weight loss. If metal is removed from the specimen by corrosion, the amount of metal can be determined by weighing the specimen before and after exposure. This has some advantages and equally important disadvantages. Weight loss can be determined very easily, very accurately with relatively unsophisticated instruments. On the other hand weight loss is a valid measure of corrosion only if corrosion is perfectly uniform [49]. Another disadvantage of the use of weight loss method for assessing corrosion damage is that the corroding metal has a film of corrosion products. To weigh the remaining metal accurately it is necessary to remove the corrosion products without removing any solid metal. This is difficult to achieve at times [49]. The data is presented in the form of a plot of weight loss/unit area versus time. This method is particularly not suitable for the study of MMC where localized attack is the process of corrosion. Moreover, the cleaning procedure may detach the reinforcing phase from the matrix. All these may lead to erroneous conclusions regarding the corrosion resistance of composites. This type of test is therefore normally conducted along with some other technique as a confirmatory test. A typical weight loss versus time plot for LM11 matrix reinforced particles and fibers in 3% NaCl solution is shown in Figure 6 [45]. It is seen that the base alloy showed the least weight loss while the composites dispersed with SiC fibers showed the most material
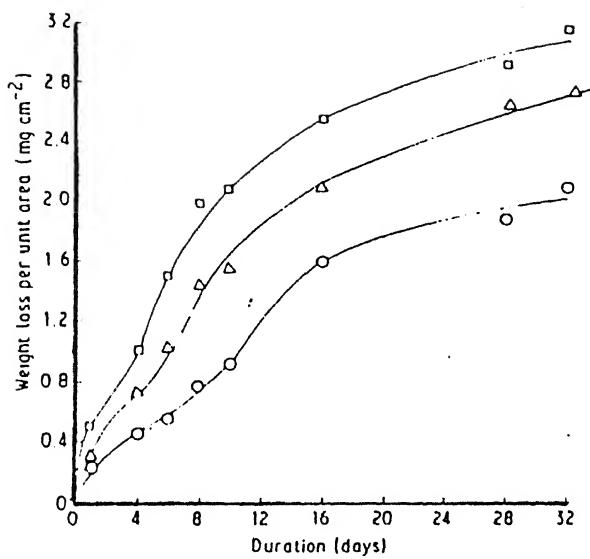
Figure 6. Weight loss as a function of exposure time for LM11 reinforce with SiC reinforcements in an immersion test in 3% NaC solution.

loss. The incubation period shown in the curve refers to the initial period required for the oxide film to breakdown in the presence of chloride ions. Shorter incubation time observed in the case of composites is attributed to the large interfacial area due to the presence of dispersoids which, in turn, initiate corrosion. The reduction in the rate of material loss at longer times is due to the accumulation of reaction products like $Al(OH)_3$ on the surface, which retard the inward diffusion of chloride ions, thereby preventing further corrosion. The following expression can be used to convert corrosion weight loss data to mils penetration per year (mpy) [49]

$$Corrosion\ rate\ (mpy) = \frac{534.W(mg)}{\rho(g/cm^3).A(in^2).t(hrs)}$$

where W is the weight loss, ρ is the specimen density, A is the specimen area and t is the exposure time.

2.7.1.2 Electrochemical polarization techniques:

In electrochemical corrosion testing two direct approaches are apparent: Control the current (i.e.,corrosion rate) and measure the resulting potential, or control the potential (i.e.,oxidizing power) and measure the resulting current. In each case the potential of an electrode in a conducting media is changed by the flow of current in the electrolytic cell. This change in potential from a reversible or steady state value as a result of current flow is known as polarization. The anodic polarization (Figure 7) represented by a metal dissolution reaction ($M \longrightarrow M^{2+} + 2e^-$) is predominant at potentials more
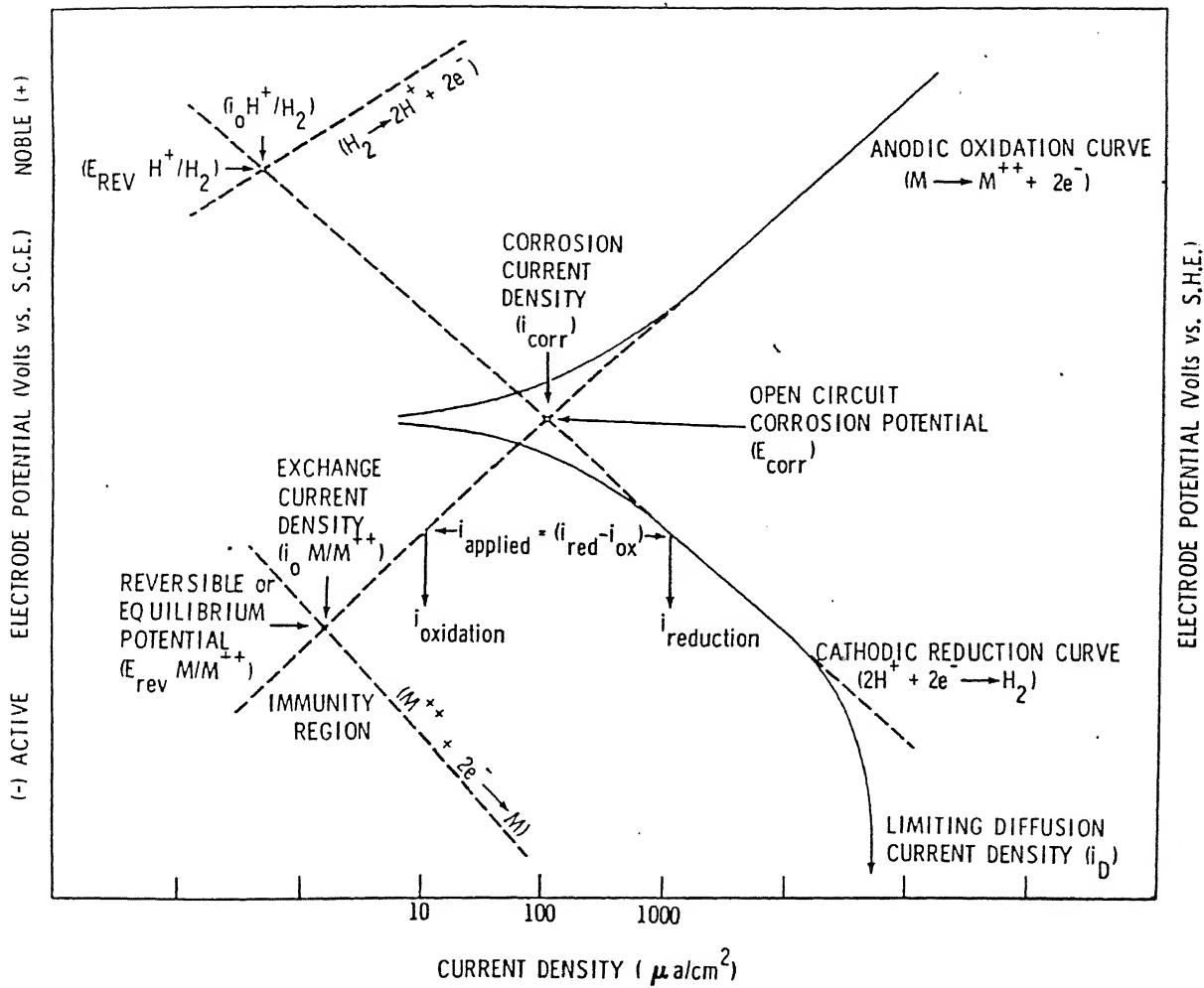
Figure 7. Schematic representation of theoritical and experimental activation polarization curves for a metal.

positive (noble) than the specimen's stabilized open circuit potential (E_{corr}), and the cathodic polarization represented by the reduction reaction ($2H^+ + 2e^- \longrightarrow H_2$) is predominant at potentials more negative (active) than E_{corr}. Activation, concentration and resistance polarization are the three fundamental types of anodic and cathodic polarization. Under activation polarization the reaction sequence at the metal-reinforcement interface controls the electrochemical process (Example:corrosion in relatively concentrated acid). Under activation control, the anodic and cathodic data for potential versus logarithm of applied current density give linear behavior when the amount of polarization, which is called overvoltage, is more than about 50 mV from E_{corr}. For the anodic curve the dashed line of Figure 7 represents the corrosion rate variation with potential. The deviation of the observed curve (solid line) from the theoretical at potentials within 50 mV of the corrosion potential is due to the fact that applied current density ($i_{applied}$) is the absolute difference between the total oxidation current density (i_{ox}) and total reduction current density (i_{red}). Near the intersection of the oxidation and reduction curves, this subtraction is significant, but at about 50 mV beyond the intersection potential, for cathodic curves $i_{applied} = i_{red}$; for anodic curves $i_{applied} = i_{ox}$ and $i_{ox} = i_{corr}$ at each potential 50 mV noble than E_{corr} as long as corrosion is the predominant oxidation reaction.

When the reaction rates are controlled by the diffusion of species in the bulk electrolyte to the metal-electrolyte interface, concentration polarization is observed. This behavior usually occurs when the concentration of the reducible species in the environment is small;for example, corrosion in aerated solutions. In such cases there is a precipitous change in potential at the limiting diffusion current density as illustrated in Figure 7. Resistance polarization can arise from an IR potential drop during electrochemical measurements in low conductivity solutions. This phenomenon has not been a serious factor in corrosion studies.

The solid polarization curves in Figure 7 which can be obtained by polarizing the specimen is curved at low overpotentials but becomes linear at high overpotentials. This linearity on a semi-log plot is termed as Tafel behavior, after the german scientist who first explained it. Extrapolation of the Tafel behavior region gives corrosion rate, I_{corr} at E_{corr}. So, this technique is also called as Tafel extrapolation technique.

Generally, polarization is done galvanostatically or potentiodynamically. In galvanostatic method current is increased at regular intervals and the resulting specimen potential is measured after it reaches a steady state value. This technique is suitable for both anodic and cathodic polarization measurements. About 50 mV from the E_{corr}, the curves exhibit linear behavior in accordance with the Tafel equation

$$\eta = \pm \beta \ln i/i_o$$

where η is the overvoltage, β is the volts/decade slope, i is the applied current density, i_o is the exchange density at the reversible potential. The length of this straight line segment of experimental curves can vary from essentially nothing to about 3 decades. The deviation from linearity at higher current densities is generally due to concentration or resistance effects. Experimental efforts are often made to maximize the linear behavior since corrosion rate at corrosion potential is determined by extrapolating the Tafel line back to E_{corr} or zero overvoltage. In case of concentration polarization, stirred or flowing electrolyte and rotating electrodes tends to minimize concentration effects. If resistance effects are the reason, a Wheatstone bridge modification of the galvanostatic circuit has been found to compensate for solution resistance. So, on such occasions where it is not always possible to obtain a linear extrapolatable Tafel line a standard method of extrapolating from a fixed current density can also be employed. Various mathematical techniques like small potential approximation, large potential approximation and three-point method are also available for obtaining I_{corr} from the polarization data [50]

Potentiodynamic polarization tests are designed to determine an overall corrosion rate profile for a metal-electrolyte system over some potential range. The electrode potential is changed at a regular step rate or sweep rate with a potentiostat and the associated current is recorded or plotted.

From Figure 7 it can be seen that the value of I_{corr} at E_{corr} can be determined either from anodic part or cathodic part or from both the parts of the polarization curves [51]. Anodic polarization results in extensive corrosion of the sample especially when carried out for extended period and the test becomes destructive in such cases. So, by polarizing the specimens cathodically alone I_{corr} values can be determined using any one of the above said techniques.

2.8 Oxidation of MMC:

It is well known that apart from influencing the mechanical properties, oxide dispersions in metallic matrix can significantly affect the oxidation behavior of alloys. Oxide scales formed on ODS alloys at high temperature possess better spallation resistance than scales formed on conventional cast or wrought alloys of the same composition [52]. For example, isothermal as well as cyclic oxidation tests conducted on Co-10%Cr-1%Al alloy with internally oxidized Al_2O_3 dispersoids shows an improved oxide adhesion because of the presence of Al_2O_3 dispersions [53]. Common reactive metal oxides like yittria and thoria not only improve scale adherence but also reduce the oxide growth rate and enhances selective oxidation. Several reasons has been put forward for the improved scale adherence. They are [53]

(1) Pegging effect: The reactive element oxidizes internally ahead of the scale-metal interface to generate an oxide dispersion. These oxide particles promote the formation of intrusions of the external oxide in to the metal called `pegs'. These pegs

From Figure 7 it can be seen that the value of I_{corr} at E_{corr} can be determined either from anodic part or cathodic part or from both the parts of the polarization curves [51]. Anodic polarization results in extensive corrosion of the sample especially when carried out for extended period and the test becomes destructive in such cases. So, by polarizing the specimens cathodically alone I_{corr} values can be determined using any one of the above said techniques.

2.8 Oxidation of MMC:

It is well known that apart from influencing the mechanical properties, oxide dispersions in metallic matrix can significantly affect the oxidation behavior of alloys. Oxide scales formed on ODS alloys at high temperature possess better spallation resistance than scales formed on conventional cast or wrought alloys of the same composition [52]. For example, isothermal as well as cyclic oxidation tests conducted on Co-10%Cr-1%Al alloy with internally oxidized Al_2O_3 dispersoids shows an improved oxide adhesion because of the presence of Al_2O_3 dispersions [53]. Common reactive metal oxides like yittria and thoria not only improve scale adherence but also reduce the oxide growth rate and enhances selective oxidation. Several reasons has been put forward for the improved scale adherence. They are [53]

(1) Pegging effect: The reactive element oxidizes internally ahead of the scale-metal interface to generate an oxide dispersion. These oxide particles promote the formation of intrusions of the external oxide in to the metal called `pegs'. These pegs

mechanically anchor the external scale to the alloy and arrest cracks propagating along the metal-oxide interface.

(2) The internally oxidized particles act as sinks for the vacancies generated as a result of scale forming process, which would otherwise condense at metal-scale interface leading to scale separation.

(3) The poor adhesion of the scale to the substrate is due to the presence of impurities like sulfur. The reactive element getters the impurity. Alternatively the impurity is gettered by the interface between the dispersed oxide particles and the matrix.

(4) In alumina forming alloys, yittrium additions leads to maintenance of fine-grained oxide by segregating to oxide grain boundaries and retarding grain boundary migration. In these fine-grained scales growth stresses can be more effectively relieved.

On pure Al, the oxide film is impervious to oxygen and the rate of growth is governed by the rate of diffusion of Al through the oxide film which leads to parabolic growth kinetics. In Al-Mg alloys which mostly is the matrix for Al-SiC and Al-Al_2O_3 composites, at temperatures above $350^{o}C$ the oxide film formed soon becomes Mg rich because the activation energy for diffusion is lower for Mg than Al in both the metal and the oxide film [54]. Once the outer surface becomes entirely covered with MgO, the situation is then thermodynamically and kinetically favorable for the reduction of Al_2O_3 by outwardly diffusing Mg to form the spinel $MgAl_2O_4$. So, a similar oxidation behavior is expected in MMC

reinforced with particulates. High temperature oxidation studies corelating scale growth rate or scale adherence to addition of particulate reinforcements has not been reported in literature.

The objective of this thesis is to study the environmental effects, especially, corrosion and hydrogen embrittlement characteristics of $Al-Al_2O_3$ particulate reinforced composites.

References:

1. I.A.Ibrahim, F.A.Mohammed and E.J.Lavernia, Particulate reinforced metal matrix composites- a review, J.Mater.Sci., 26, 1137 (1991).

2. A.K.Ghosh, Processing of Metal Matrix Composites, ed.R.Trivedi, J.A.Sekhar and J.Mazumdar in "Principles of Solidification and Materials Processing", p585, Oxford and IBH Publication.Co., India (1989).

3. N.G.Nicholas, Ceramic-Metal Interfaces, ed.L.C.Dufor *et al.*, in "Surfaces and Interfaces of Ceramic Materials", p393, Kulver Academic Publishers (1989).

4. T.W.Clyne and P.J.Withers, "An Introduction to Metal matrix Composites", p193, Cambridge University Press (1993).

5. V.Laurent, D.Chatain, C.Chatillon and N.Eustathopoulos, Wettablity of mono crystalline alumina by aluminium between its melting point and 1273K, Acta Metall., 36, 1797 (1988).

6. R.B.Bhagat,Casting Fiber Reinforced Metal matrix Composites, ed.R.K.Everett and R.J.Arsenault,"Metal Matrix Composites", p46, Academic Press, New York (1991).

7. B.F.Quigley, G.J.Abbaschian, R.Wunderlin and R.Mehrabian, A Method for Fabrication of Aluminium-Alumina Composites, Met Trans., 13A, 93 (1982).

8. C.G.Levi, G.J.Abbaschian, and R.Mehrabian, Interface Interactions During Fabrication of Aluminium Alloy-Alumina Fiber Composites, Met Trans., 9A, 697 (1978).

9. P.K.Ghosh and Subrata Ray, Influence of Holding Temperature

and Stirring Speed on the Surface Reaction Layer on Al_2O_3 Particles Embedded in Compocast Al-Mg Alloy, Z.Metallkde, 81, 525 (1990).

10. P.K.Ghosh and S.Ray, Fabrication and Properties of Compocast Aluminium-Alumina Particulate Composite, Indian Journal of Technology, 26, 83 (1988).

11. B.C.Pai, Subrata Ray, K.V.Prabhakar and P.K.Rohatgi, Fabrication of Aluminium-Alumina (Magnesia) Particulate Composites in Foundries using Magnesium Additions to the Melts, Matl.Sci.and Eng., 24, 31 (1976).

12. P.K.Rohatgi, R.Asthana and S.Das, Solidification, structures, and properties of cast metal-ceramic particle composites, Int.Met.Rev., 31, 115 (1986).

13. J.C.Viala, P.Forter and J.Bouix, Stable and meta stable phase equilibria in the chemical interaction between aluminium and silicon carbide, J.Mater.Sci., 25, 1842 (1990).

14. A.Banerji and P.K.Rohatgi, Cast Al Alloy Containing Dispersions of TiO_2 and ZrO_2 particles, J.Mater.Sci., 17, 335 (1982).

15. D.J.Lloyd, Particle Reinforced Composites Produced by Molten Metal Mixing, ed.S.K.Das, C.P.Ballard and F.Marikar, in "High Performance Composites for the 1990's", 33, The Minerals, Metals, & Materials Society, Warrendale, (1991).

16. M.Vogelsang, R.J.Arsenault and R.M.Fisher, An *in-situ* HVEM Study of Dislocation Generation at Al/SiC Interfaces in Metal Matrix Composites, Met.Trans., 17A, 379 (1986).

17. M.Taya, K.E.Lulay and D.J.Lloyd, Strengthening of a Particulate Metal Matrix Composite by Quenching, Acta Metall., 39, 73 (1991).

18. R.J.Arsenault, L.Wang and C.R.Feng, Strengthening of Composites due to Microstructural Changes in the Matrix, Acta Metall., 39, 47 (1991).

19. T.Christman and S.Suresh, Microstructural Developments in an Al Alloy-SiC Whisker Composite, Acta Metall, 36, 1691 (1988).

20. M.V.Ravichandran, R.Krishna Prasad and E.S.Dwarakadasa, Fracture Toughness Evaluation of Aluminium 4% $Mg-Al_2O_3$ Liquid-Metallurgy Particle Composite, J.Mater.Sci.Let., 11, 452 (1992).

21. P.K.Ghosh, P.R.Prasad and S.Ray, Effect of Porosity on the Strength of Particulate Composites, Z.Metallkde, 75, 934 (1984).

22. P.K.Ghosh, S.Ray and P.K.Rohatgi, Incorporation of Alumina Particles in Aluminium-Magnesium Alloy by Stirring in Melt, Trans. Jap.Inst.Met., 25, 440 (1984).

23. P.K.Ghosh and S.Ray, Effect and Alumina Content on the Mechanical Properties of Compocast Aluminium Alloy-Alumina Particulate Composite, J.Mater.Sci., 21, 1667 (1986).

24. P.K.Ghosh and S.Ray, Effect and Alumina Content on the High Temperature Mechanical Properties of Compocast Aluminium Alloy-Alumina Particulate Composite, J.Mater.Sci., 22, 4077 (1987).

25. S.Ray, Process Development for Fabrication of Cast Metal

Matrix Particulate Composite : Unsolved Problems, Trans.Indian.Inst.Met., 45, 69 (1992).

26. J.W.Watson,Y.Z.Shen and M.Meshii, Effect of Cathodic Charging on the Mechanical Properties of Aluminium, Met.Trans., 19A, 2299 (1988).

27. M.O.Speidel, Hydrogen Embrittlement of Aluminium Alloys ?, ed.I.M.Bernstein and A.W.Thompson, in "Hydrogen in Metals", p249, ASM (1974).

28. D.A.Jones,"Principles and Prevention of Corrosion", p334, Maxwell Macmillan International Publishing Group, New York (1992).

29. G.M.Pressouyre, Trap Theory of Hydrogen Embrittlement, Acta Metall., 28, 895 (1980).

30. G.M.Pressouyre and I.M.Bernstein, A Kinetic Trapping Model for Hydrogen-Induced Cracking, Acta Metall., 27, 89 (1979).

31. R.Gibala and D.S.DeMiglio, Hydrogen in Iron and Steels: Interactions, Traps, and Crack Paths, ed.I.M.Bernstein and A.W.Thompson, in "Hydrogen Effects in Metals", p113, The Metallurgical Society of AIME, Warrendale, (1981).

32. G.M.Pressouyre and I.M.Bernstein, A Quantitative Analysis of Hydrogen Trappings, Met.Trans., 9A, 1571 (1978).

33 R.A.Oriani and P.H.Joseph, Equilibrium Aspects of Hydrogen Induced Cracking in Steels, Acta Metall., 22, 1065 (1974).

34. R.A.Oriani and P.H.Joseph, Equilibrium and Kinetic Studies of Hydrogen Assisted Cracking of Steels, Acta Metall., 25, 979 (1977).

35. A.N.Stroh, A Theory of Fracture of Metals, Adv in Phy., 6, 418 (1957).

36. C.D.Beachem, A New Model for Hydrogen Assisted Cracking (Hydrogen embrittlement), Met.Trans., 3, 437 (1972).

37. H.K.Birnbaum, Hydrogen Embrittlement of Molybdenum, Scripta Metall., 9, 1113 (1975).

38. H.K.Birnbaum, Low Temperature Hydrogen Embrittlement of Nb II: Microscopic Observations, Acta Metall., 25, 135 (1977).

39. X.Y.Huang, W.Mader and R.Kirchheim, Hydrogen and Oxygen at Metal/Oxide Interfaces, Acta Metall., 39, 893 (1991).

40. Govind, R.Balasubramaniam and G.S.Upadhyaya, Effect of Hydrogen on Ductility of ODS Copper, Scripta Metall. Mater., 29, 1303 (1993).

41. D.M.Aylor and P.J.Moran, Effect of Reinforcement on the Pitting Behavior of Aluminium-Base Metal Matrix Composites, J.Electrochem.Soc., 132, 1277 (1985).

42. M.Saxena, B.K.Prasad and T.K.Dan, Corrosion Characteristics of Aluminium Alloy Graphite Composite in Various Environments, J.Mater.Sci., 27, 4805 (1992).

43. M.S.N.Bhat, M.K.Surappa and H.V.Sudhaker Nayak, Corrosion Behavior of Silicon Carbide Particle Reinforced 6061/Al Alloy Composites, J.Mater.Sci., 26, 4991 (1991).

44. R.C.Paciej and V.S.Agarwala, Influence of Processing Variables on the Corrosion Susceptibility of Metal-Matrix Composites, Corrosion Science, 44, 680 (1988).

45. O.P.Modi, M.Saxena, B.K.Prasad, A.H.Yagneswaran and

M.L.Vaidya, Corrosion behavior of squeeze-cast aluminium alloy - silicon carbide composites, J.Mater.Sci., 27, 3897 (1992).

46. Deo Nath and T.K.G. Namboodhiri, Some corrosion characteristics of aluminium - mica particulate composites, Corrosion Science, 29, 1215 (1989).

47. H.Sun, E.Y.Koo and H.G.Wheat, Corrosion behavior of SiC_p/6061 Al Metal Matrix Composites , Corrosion , 47, 741 (1991).

48. M.Saxena, O.P.Modi, A.H.Yagneswaran and P.K.Rohatgi, Corrosion characteristics of cast aluminium alloy - 3 Wt% Graphite particulate composites in different environments, Corrosion Science, 27, 249 (1987).

49. W.H.Ailor," Handbook of corrosion testing and evaluation ", p174, John Wiley and Sons Inc, New York (1971).

50. S.Barnartt, Electrochemical Nature of Corrosion, ed., R.Baboian in "Electrochemical Techniques for Corrosion", p3, NACE, Texas (1977).

51. S.W.Dean, Electrochemical Methods of Corrosion Testing, ed., R.Baboian in "Electrochemical Techniques for Corrosion", p52 NACE, Texas (1977).

52. W.J.Quadakkers, H.Holzbrecher, K.G.Briefs and H.Beske, Differences in Growth Mechanisms of Oxide Scales Formed on ODS and Conventional Wrought Alloys, Oxidation of Metals, 32, 67 (1989).

53. L.M.Kingsley and J.Stringer, The Effect of an Al_2O_3

Dispersion on the Adhesion of Al_2O_3 Scales on Alumnized Co-10%Cr Alloys, Oxidation of Metals, 32, 371 (1989).

54. C.Lea and J.Ball, The Oxidation of Rolled and Heat-Treated Al-Mg Alloys, Applications of Surface Science, 17, 344 (1984).

CHAPTER 3

EXPERIMENTAL PROCEDURE

The experimental part of the thesis includes preparation of Al-Al_2O_3 particulate reinforced composites, their characterization, study of their corrosion behavior in HCl environment and assessment of the effect of hydrogen charging on their mechanical properties.

3.1 Preparation of Al-Al_2O_3 Particulate Reinforced Composites:

The liquid-metallurgy technique which is more direct and simpler compared to other processes was adopted in preparing composites. The furnace used was a resistance heated box type furnace with SiC heating elements (Figure 8). A calibrated Platinum- Rhodium thermocouple was inserted through the top cover of the furnace so that its tip remained just above the melt surface. 1000g commercial pure Al was melted and super heated to 1148 K (875°C) in a clay graphite crucible. This superheated melt was taken out of the furnace and degassed using hexachloroethane tablets. The dross was skimmed out before Mg addition was made. 10 Wt% Mg, which was weighed and wrapped in thin Al sheet was introduced in to the melt. Wrapping in Al sheet improves Mg recovery. Once the Mg had melted completely, the crucible was taken to the stirring unit where a stirrer (with a mixing head as shown in Figure 9) was dipped in to the melt. The d/D ratio and h/H ratios were 0.48 and 0.78 respectively; where D is the diameter of the crucible, d is the diameter of the stirrer, h is the position of the stirrer from the bottom of the crucible and H
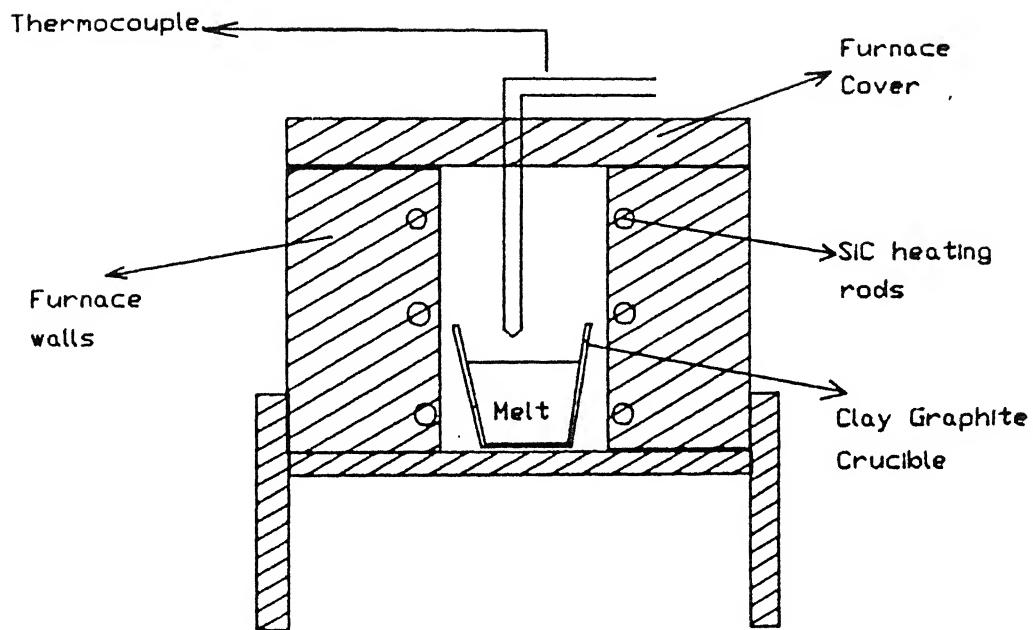
Figure 8. Schematic diagram of the furnace setup used for melting
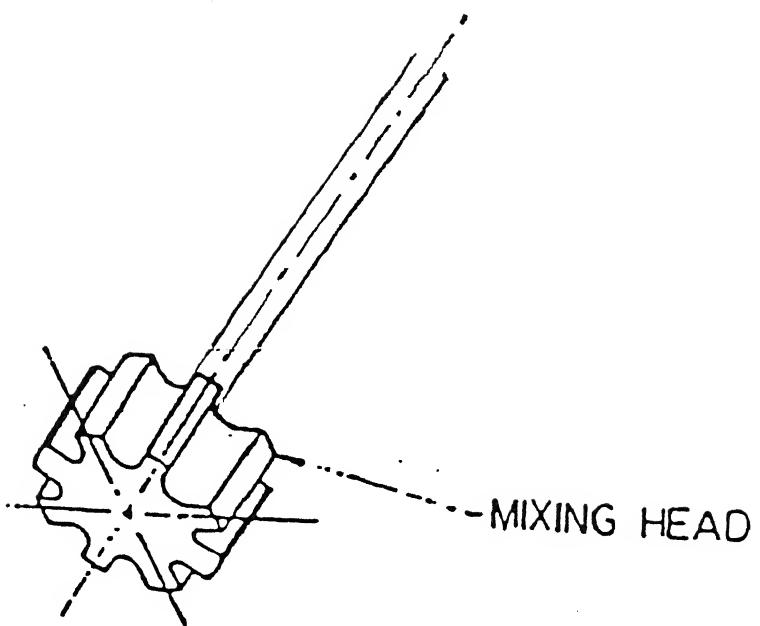
Figure 9. Schematic diagram of the mixing head of the stirrer

is the depth of the melt in the crucible. The stirrer used was coated with a mixture of graphite powder and sodium silicate and was dried properly in an oven before using it for stirring. After the immersion of the stirrer of the stirrer in the melt, the speed of the stirrer was gradually increased to 450 rpm. Irregular shaped acicular α-Al_2O_3 particles in the size range 100-150 microns obtained by sieving (Figure 10) were preheated to 873K (600°C) before dispersing them in the melt. As the stirrer speed picked up and as soon as the vortex started forming in the melt, preheated Al_2O_3 particles were gradually added manually to the vortex. Stirring was continued for another half-a-minute (approximately) after all the particles are added and the melt was immediately cast in a permanent metallic mold. After the solidification process was complete and the ingot had cooled down to room temperature, the piped regions of the ingots were cut and discarded. Specimens for subsequent testing were obtained from the bottom of the ingots.

Similar runs were carried out incorporating 2,4 and 8 Wt% of Al_2O_3 keeping the Mg content constant at 10 Wt%. A reference material with 0% Al_2O_3 was also cast so that properties of Al_2O_3 reinforced composites can be compared with that of the base material without reinforcement and the effect of Al_2O_3 additions could be understood. A high Mg recovery is expected for the base material without reinforcement since this melt was not to be stirred. Therefore in order to maintain a uniform Mg concentration in all the melts a reduced amount of only 7 Wt% Mg was added while

Figure 10.   Size distribution and shape of Al_2O_3 particles used.

casting the reference material. This assumes a 30-40% loss of Mg due to stirring while preparing the composites.

3.2 Characterization:

3.2.1 Microscopy:

The composites prepared by liquid metallurgy route were cut and pieces and pieces of them were mounted using a cold setting resin. The specimens were polished with SiC emery papers up to 4/0 and were finally cloth polished using 1, 0.3 and 0.05μm Al_2O_3 powder. The polished specimens were then studied under an optical microscope (CARLZEISS-JENA) to observe the distribution of the reinforcing second phase. The specimens used for Scanning Electron Microscopy (JEOL, JSM 840A)were coated with silver. Compositional spot analyses were performed in and around the particles to characterize the interface between the particle and the matrix.

3.2.2 Hardness Measurement:

Vickers microhardness testing was carried out after polishing the specimens using a micro hardness tester (CARLZEISS-JENA)using a 20 gram load. Indentations were taken at varying distances from the interfaces of the reinforcing phase so as to assess the effect of reinforcing phase on the hardness of the matrix.

3.3 Hydrogen Embrittlement Studies:

Tensile testing of hydrogen pre-charged specimens were conducted to assess the effect of hydrogen on the mechanical properties of $Al-Al_2O_3$ particulate reinforced composites. Tensile test specimens were machined from the bottom of the cast ingots. The dimensions of the specimen are shown in Figure 11. The
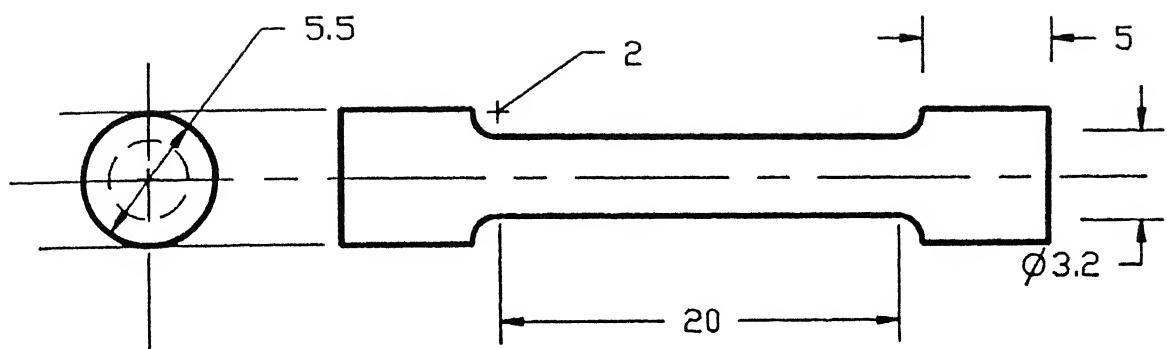
All dimensions in mm

Figure 11. Goemetry of the tensile test specimens used in hydrog
charging tests.

specimens were degreased and cleaned with acetone before hydrogen charging. The electrolyte used for hydrogen charging was 1N H_2SO_4. The specimen grips were covered with Teflon tape to prevent hydrogen charging in the grips. The specimens were made cathode and a stainless steel strip was used as anode in the electrochemical cell. A few drops of sodium arsenite, a hydrogen re-combinant poison, were added to the H_2SO_4 solution to inhibiting the formation of molecular hydrogen thereby accelerating the entry of hydrogen in to the material. The current density during charging was kept constant at 50 mA/cm^2 All the specimens were charged for a period of 12 hours. After hydrogen charging the specimens were cleaned and tensile tests were performed immediately. Tests were also conducted on uncharged specimens to obtain reference properties. The specimens were tested in an Instron testing machine (Model 1199). In all the cases the strain rate was kept constant at 4×10^{-5}/Sec. Engineering stress-strain curves were obtained from the load-elongation plots. The %Elongation, up to UTS was used for calculating %ductility loss for each condition using the formula

$$\% \text{ Ductility loss} = \frac{E_u - E_c}{E_u}$$

where E_u and E_c are %Elongation up to UTS for the reference and hydrogen charged specimens.

The fracture surfaces of the reference and hydrogen charged specimens (which were stored in a desiccator after testing) were later observed using Scanning Electron Microscope. The specimens

were coated with silver before the observation. The imaging was done using secondary electrons to get a better topological contrast.

3.4 Corrosion Studies:

One of the most common methods of assessing corrosion damage is by finding out the weight loss in the corrosion medium. This technique is valid if the corrosion is uniform over the surface [1] which ,incidentally, is not the case in the corrosion of composites [2-5]. On composites, the oxide film is discontinuous and these discontinuities at the reinforcement-matrix interface initiate corrosion. Moreover weight loss measurements are time consuming. A more quicker and accurate method of testing is by the Tafel extrapolation method employing galvanostatic or potentiodynamic polarization. A vibrant potentiostat (Model VSM/M/30)was used for conducting the polarization (Tafel extrapolation) experiments. Test specimens of area 1 cm^2 were mounted in epoxy allowing for electrical contact with the mounted specimen. They were polished down to 4/0 emery level using SiC papers and stored in a desiccator for 24 hours before the experiments. Experiments were conducted in 0.1N HCl solution at room temperature in a standard polarization cell with a platinum sheet as auxiliary electrode. The schematic of the corrosion test cell is shown in Figure 12. The open circuit potential (OCP) was monitored for a minimum period of 24 hours or until the potential was stabilized. The specimens were polarized catholically in the current range $0 \mu A$ to $5000 \mu A$ after a steady OCP was attained.
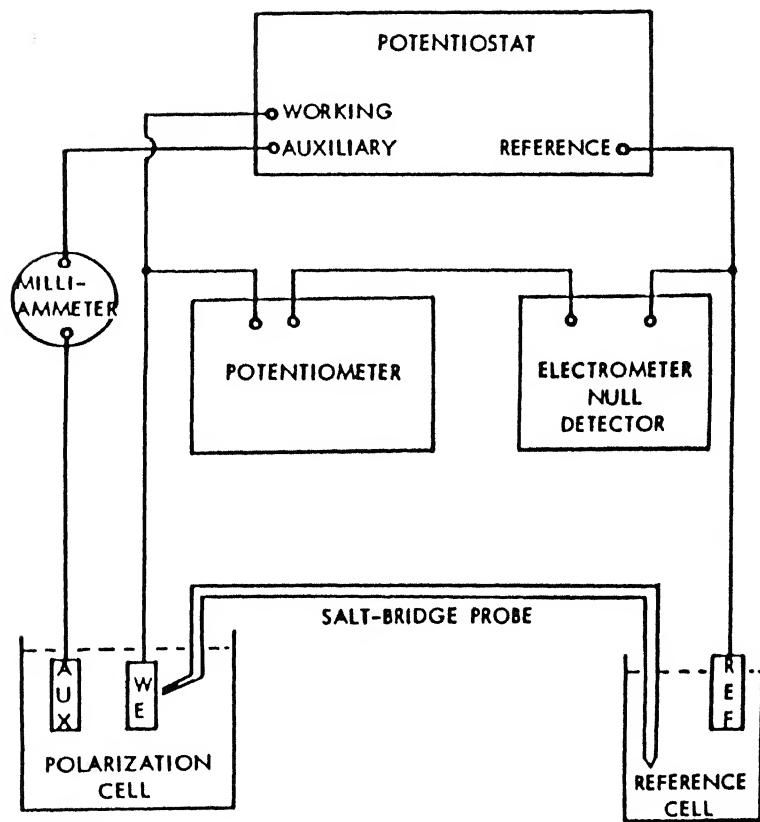
Figure 12.   Schematic diagram of the corrosion test cell.

Steady state over potentials were noted down at each applied current density. The voltages were measured with reference to a standard calomel electrode (SCE) in all the experiments. The corrosion density (I_{corr}) obtained by extrapolating the cathodic region of the polarization curve to the stabilized OCP (E_{corr})is a measure of corrosion rate [1]. The polarization curves did not exhibit a distinct extrapolatable linear portion. Therefore the extrapolation was performed from a fixed current density of $1000\mu A/cm^2$ for all the experiments

3.4.1 Thermogravimetry:

Isothermal oxidation studies were conducted with a thermogravimetric setup (shown in Figure 13) to understand the nature of oxide film covering the surface of the composites. Specimens of dimension 2cm X 1cm X 0.5cm were polished with SiC emery papers up to 4/0 and cleaned with soap solution and acetone before subjecting to high temperature oxidation. The specimens were inserted in to the hot zone of a platinum resistance furnace at 773K ($500^{o}C$) andcommercial pure oxygen purified by an elaborate gas train was passed in to this leak proof chamber. The temperature was maintained within $\pm$ 2K using a Indotherm temperature controller.Weight gain was monitored using a Cahn 1000 electrobalance and the values were recorded in a strip chart recorder as a function of time.
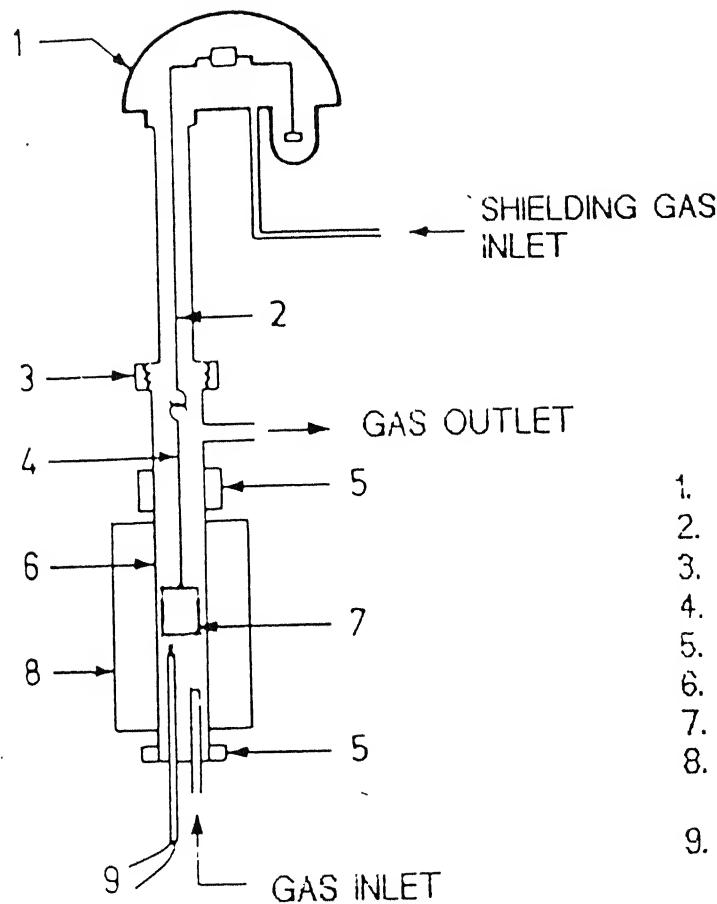
1. CAHN BALANCE
2. INCONEL ROD
3. SCREW CAP
4. HANGING ARRANGEMENT
5. COOLING ARRANGEMENT
6. ALUMINA TUBE
7. SAMPLE
8. PLATINUM–RHODIUM WOUND FURNACE
9. Pt–Pt10%Rh THERMOCOUPLE

Figure 13. Schematic diagram of the thermogravimetry setup with Cahn electrobalance

References:

1. W.H.Ailor," Handbook of corrosion testing and evaluation ", p174, John Wiley and Sons Inc, New York (1971).

2. M.S.N.Bhat, M.K.Surappa and H.V.Sudhaker Nayak, Corrosion Behavior of Silicon Carbide Particle Reinforced 6061/Al Alloy Composites, J.Mater.Sci., 26, 4991 (1991).

3. O.P.Modi, M.Saxena, B.K.Prasad, A.H.Yagneswaran and M.L.Vaidya, Corrosion behavior of squeeze-cast aluminium alloy – silicon carbide composites, J.Mater.Sci., 27, 3897 (1992).

4. Deo Nath and T.K.G. Namboodhiri, Some corrosion characteristics of aluminium – mica particulate composites, Corrosion Science, 29, 1215 (1989).

5. M.Saxena, B.K.Prasad and T.K.Dan, Corrosion Characteristics of Aluminium Alloy Graphite Composite in Various Environments, J.Mater.Sci., 27, 4805 (1992).

CHAPTER 4

RESULTS AND DISCUSSION

4.1 Microstructural study:

The typical cast microstructures of the materials under study are presented in Figure 14. The materials exhibit a certain extent of particle agglomeration and porosity which are typical of cast microstructures. Due to rigorous stirring of the degassed melt the castings contained pinhole pores. The presence of these pin hole pores in the cast structure is unavoidable because of the suction of air (along with Al_2O_3) through the vortex during stirring of the melt. It has also been reported that porosity is a function of size, position, and speed of the stirrer for a given setup and the process variables that lead to maximum incorporation of Al_2O_3 lead to maximum porosity [1,2,3]. In the present case, although the stirring assembly (size and position) and the stirring speed was maintained constant, the results of the porosity measurements conducted on these materials (Table 1 and Figure 15) indicate that higher the reinforcement fraction higher the porosity.

SEM observation of the cast microstructures revealed minute hair line cracks on some of the particles depending on the percentage addition of Al_2O_3. Although minute hairline cracks could be observed on these particles, the particles were themselves still integral. The presence of such cracked particles in the cast specimens indicates that particle cracking is not due to mechanical loading during later tensile testing or hydrogen charging. Cracking of particles due to thermal shock, as suggested

200X
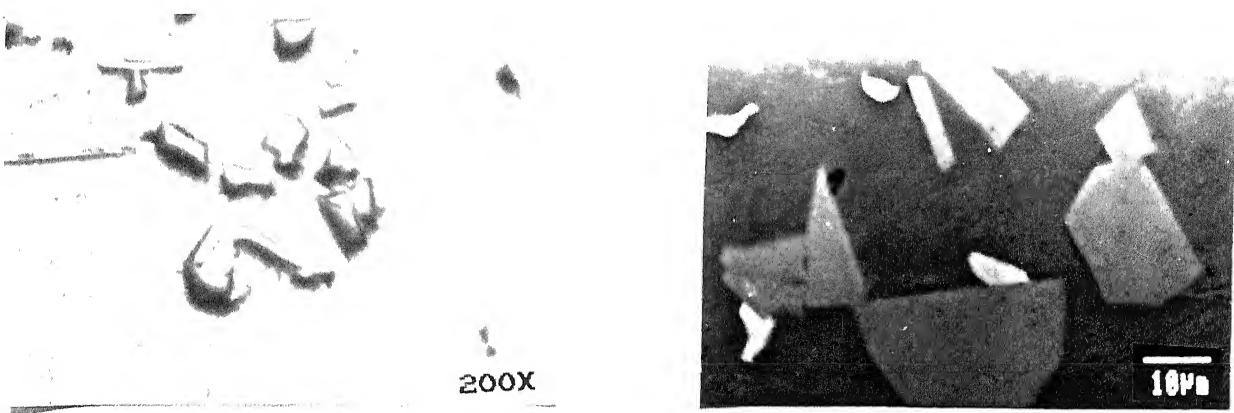
Figure 14. Typical   optical   and   SEM   microstructures   of   Al-8% Al_2O_3
composites
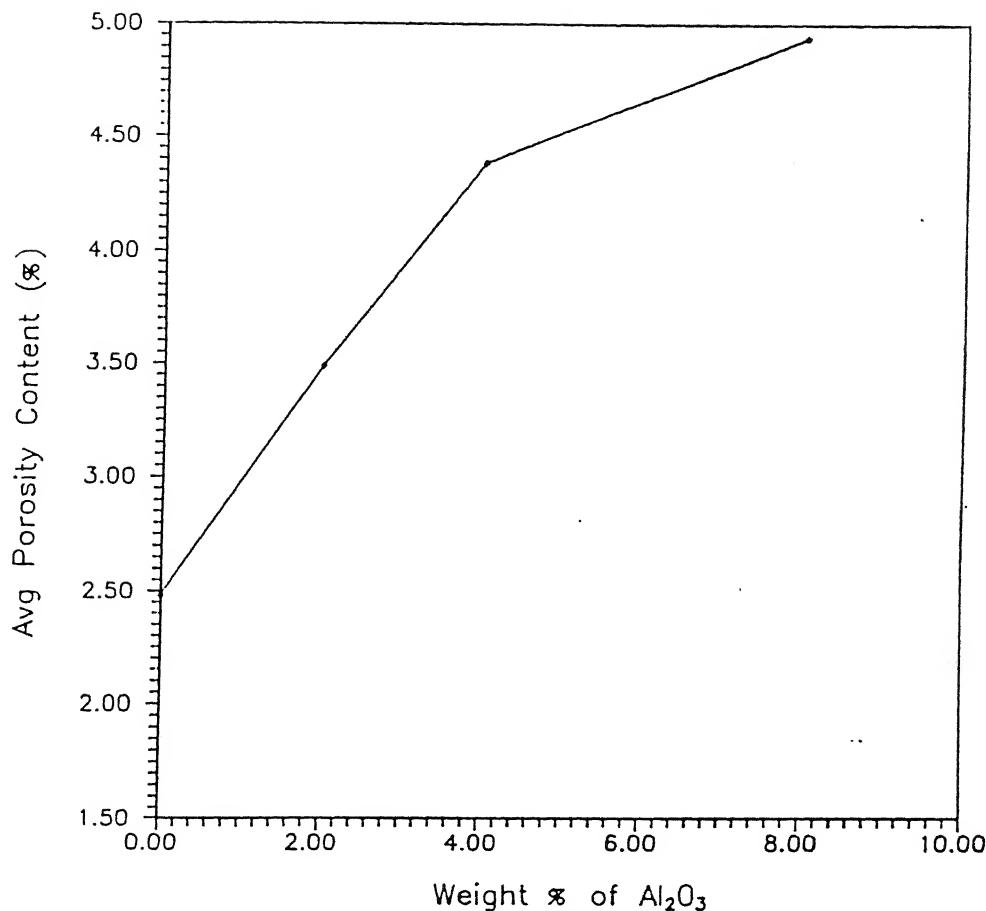
Figure 15. Variation of porosity content with Al_2O_3 volume fraction

Table 1 : Porosity content in base and composite materials

| Material	Porosity (Vol %)
Al-0% Al_2O_3	2.48
Al-2% Al_2O_3	3.49
Al-4% Al_2O_3	4.38
Al-8% Al_2O_3	4.94

in reference [4], could not have occured in this case as the particles were preheated to 873K (600°C) before incorporation in the melt. EDAX analysis on such cracked particles showed that the particle had reacted with the Mg in the matrix and had converted to $MgAl_2O_4$ (Figure 16a). The extent of conversion to $MgAl_2O_4$ was lower with increasing Al_2O_3 fraction in the composite. This conversion of Al_2O_3 particulates in Al-Mg alloys to $MgAl_2O_4$ and associated microcracking has been previously reported in the literature [1,4,5]. $MgAl_2O_4$ spinel formation occurs by any one of the following reactions [5,6]:

$$3 \ (Mg) \ + \ 4 \ [Al_2O_3] \ = \ 3 \ [MgAl_2O_4] \ + \ 2 \ (Al) \ \text{------} \ [1]$$

$$2 \ (Mg) \ + \ \{O_2\} \ = 2 \ [MgO]$$

$$2 \ [MgO] \ + \ 4 \ (Al) \ + \ 3 \ \{O_2\} \ = 2 \ [MgAl_2O_4]$$

$$\Big\} \ \text{------------} \ [2]$$
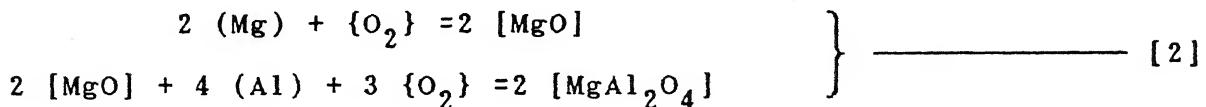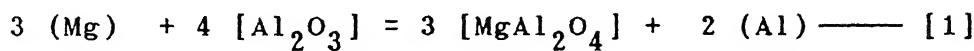
The cracking of such converted particles is due to the stresses generated to accommodate the reaction product $MgAl_2O_4$ which occupies a larger volume than does the reactant Al_2O_3. In such cases compressive stresses are generated at the particulate-matrix interface and both the particle and the surrounding matrix are subjected to compressive stresses. It is reasonable to assume that these compressive stresses cause hair line cracking of the particlulates, as has been observed in other particulate reinforced metallic systems [7]. A part of these stresses could be possibly be relieved this way and the rest could contribute to the work hardening of the adjacent matrix. As a result the matrix hardness is expected to be higher near the interface than farther away from it. This effect is verified by microhardness
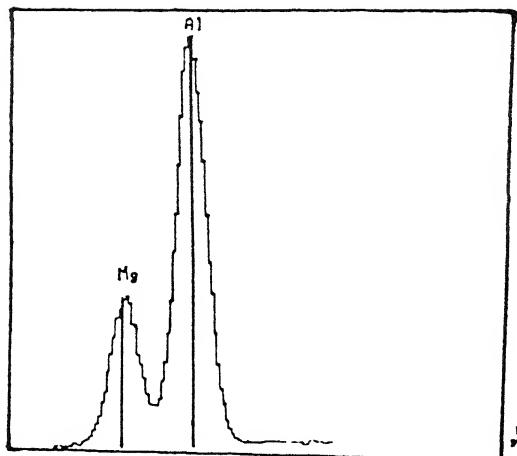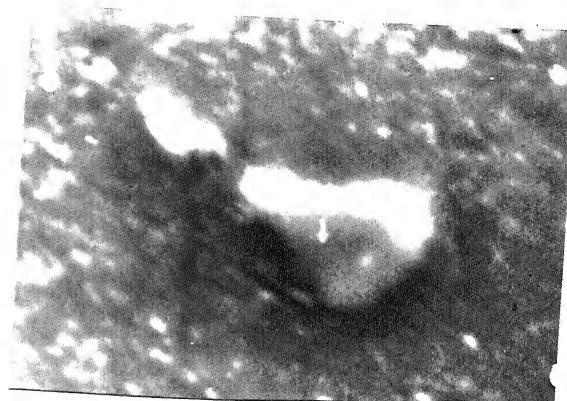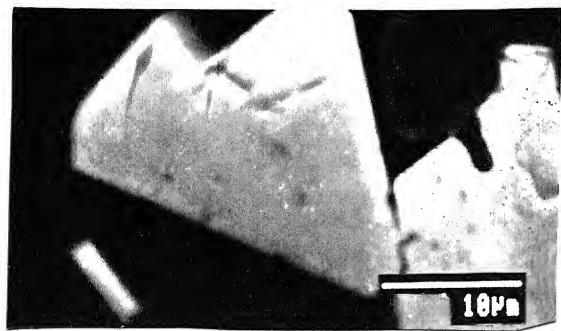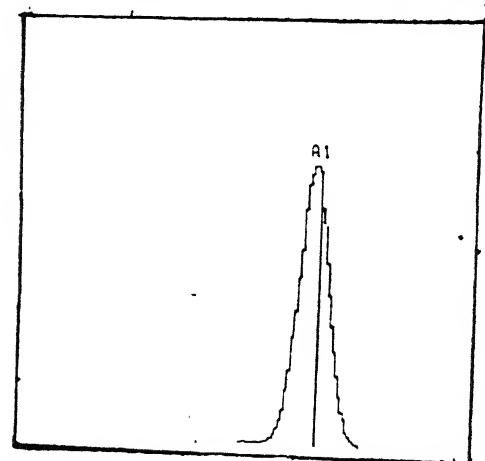
Figure 16. a) A cracked particle in Al-2% Al_2O_3 composite and ED[

analysis done on it

b) An uncracked particle in Al-8% Al_2O_3 composite and EDA)

analysis done on it.

measurements on the cast microstructures of the composites. The results of the microhardness tests conducted on a composite material ($Al-8\%$ Al_2O_3) are shown in Table 2. As expected matrix hardness at the interface is higher than that away from the interface. The number of particles that had converted to $MgAl_2O_4$ (and cracked consequently) decreases with increasing volume fraction of Al_2O_3. One such particle in $Al-8\%$ Al_2O_3 composite is shown in Figure 16b and EDAX spot analysis of its composition indicated that it was unreacted Al_2O_3.

4.2 Hydrogen Embrittlement Study:

The engineering stress-strain curves for the uncharged and hydrogen charged specimens of the base and composite materials are shown in Figure 17a and 17b. The mechanical properties obtained from these tests are tabulated in Table 3.

Ductility of the specimens (represented by % elongation) as well as UTS decreases upon hydrogen charging in all the cases. Fractographic analyses carried out on hydrogen charged and uncharged specimens showed brittle fracture characteristics in all the cases. The degree of brittleness was higher in the hydrogen charged specimens compared to uncharged specimens. Extensive particle cracking was observed on the fracture surfaces of both uncharged and charged materials (Figure 18).

4.2.1 Mechanical properties of uncharged materials:

In case of the uncharged specimens, the low ductilities observed are due to the cast structure of the materials. Reinforcement with Al_2O_3 particulates changes both UTS and

Table 2: Microhardness of the phases.

Feature	Micro-Hardness (VHN)
Al_2O_3 Particle	282.9
Interface	127.6
Matrix	95.7
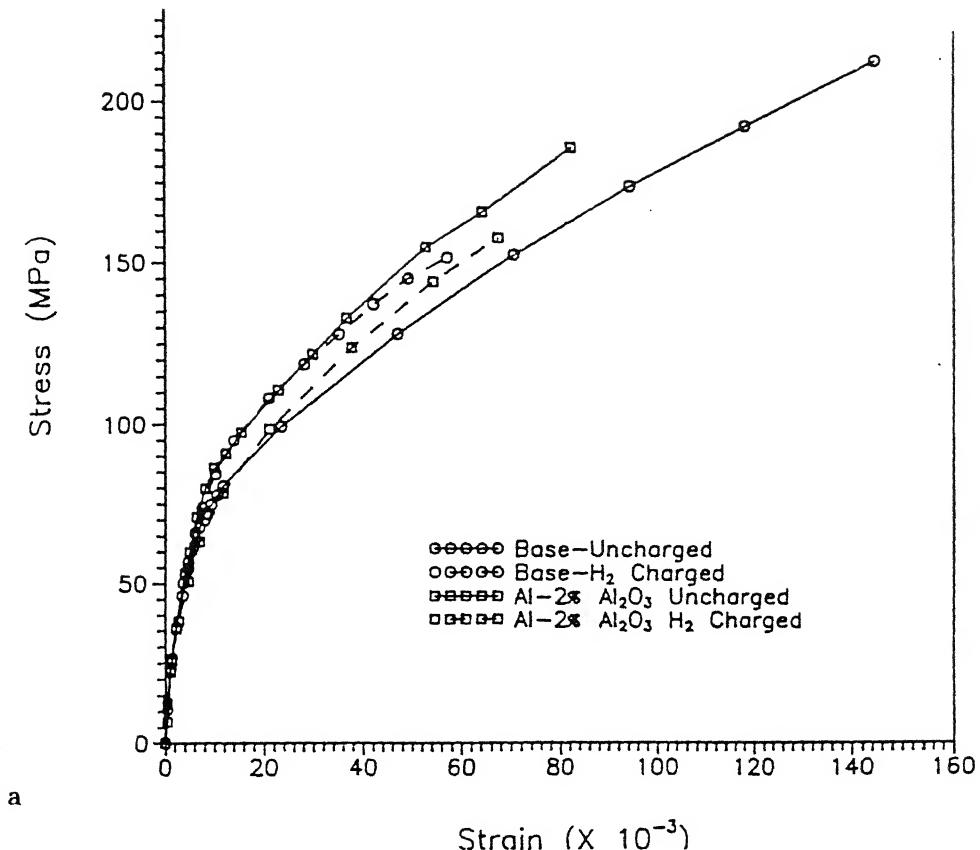
Figure 17 Engineering Stress-Strain curves of hydrogen charged and uncharged specimens. a) Base and Al-2% Al_2O_3 b) Al-4% Al_2O_3 and Al-8% Al_2O_3.
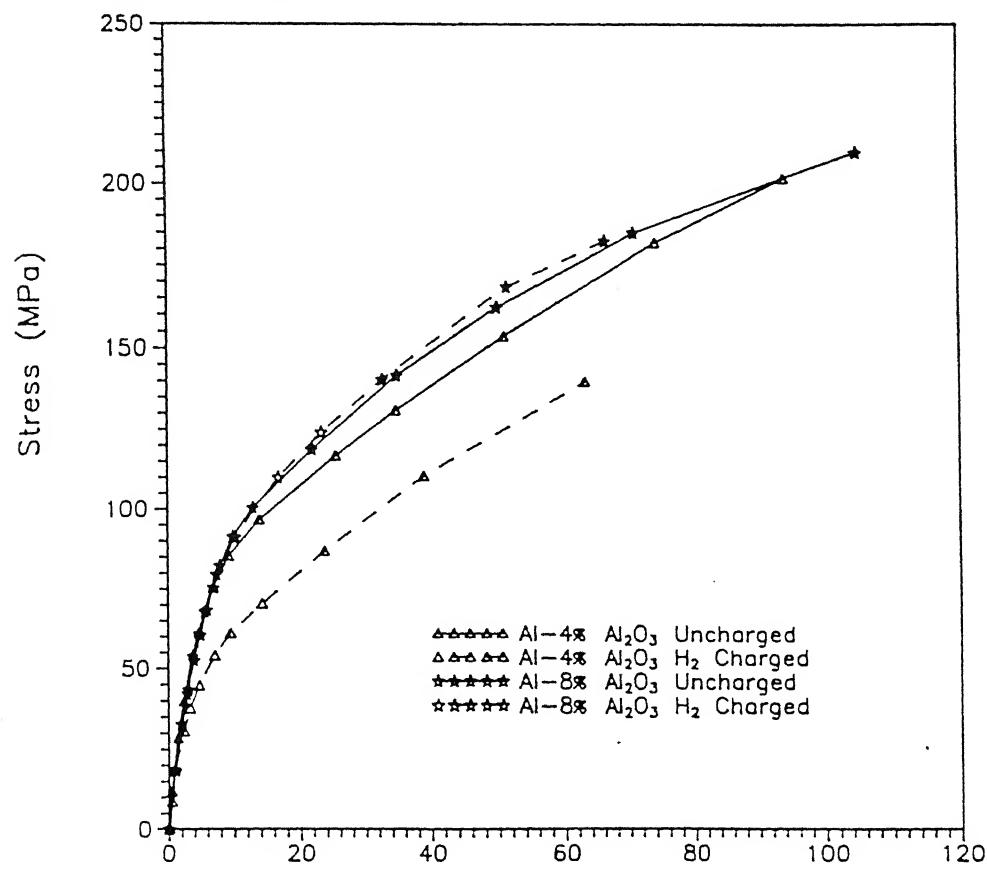
Table.3: Mechanical Properties of hydrogen charged and uncharged specimens.

Material	Uncharged		H_2 Charged		% Ductility loss
	UTS (MPa)	% Elongation	UTS (MPa)	% Elongation	
Base	212.70	13.50	151.78	5.73	57.60
Al-2% Al_2O_3	186.13	8.24	158.08	6.76	17.96
Al-4% Al_2O_3	201.83	9.42	139.72	6.33	32.80
Al-8% Al_2O_3	210.00	10.50	182.40	6.65	36.60
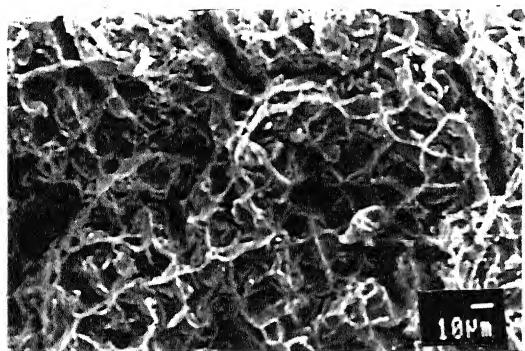
(a)
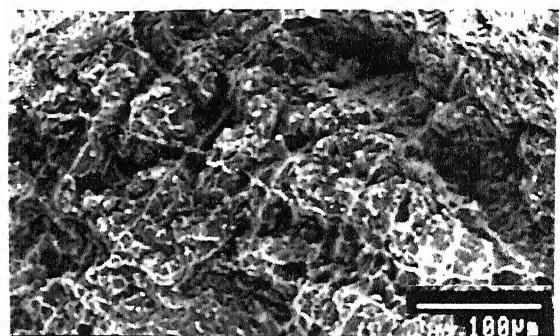
(b)

Figure 18. Fracture surfaces of charged and uncharged specimens

(a) Al-2% Al$_2$O$_3$ – Uncharged

(b) Al-2% Al$_2$O$_3$ – Hydrogen charged

ductility of the base material. UTS and percentage elongation drops to a minimum for Al-2% Al_2O_3 composite and increases thereafter with increasing reinforcement volume fraction.

The degree of conversion (i.e., the number of particles that has converted to $MgAl_2O_4$) plays a major role in deciding the mechanical properties of the composites. In this regard, the extent of conversion is decided by the Al_2O_3 content in the composite. The Mg content in the matrix of all the composites is expected to be constant since the stirring time was approximately maintained constant. So at low volume fraction of Al_2O_3 (i.e., at 2% Al_2O_3) the probability of the particles reacting and converting to $MgAl_2O_4$ is quiet high. Therefore a large number of particles crack in the case of Al-2% Al_2O_3 composite. The presence of such cracked particles weaken the integrity of the composite and the mechanical properties shows a minimum for this composite. However, a higher fraction of the particulates is retained as Al_2O_3 in composites with higher reinforcement fraction as the chemical reaction between Mg and Al_2O_3 is limited to the surface of the particulates. This results in the formation of only a thin layer of reaction product on the surfaces of the composite and provides good bonding between the matrix and the reinforcement. Additionally, this results in particulates that are essentially crack-free in the composites containing higher Al_2O_3 fractions (Figure 19). This leads to increasing strengths with increasing reinforcement fractions.

$MgAl_2O_4$

Al_2O_3

Hair line cracks
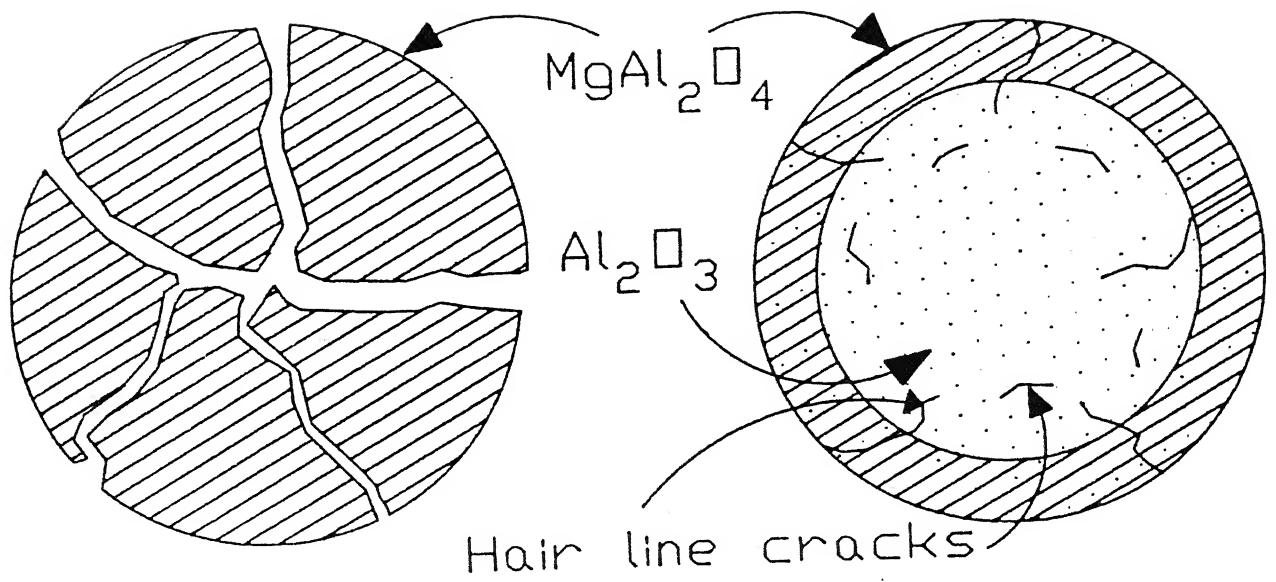
Figure 19. Schematic representation of particle cracking in Al-2% and Al-8% Al_2O_3 composite.

Another factor which affects the mechanical properties is the porosity content of the cast composites. Besides reducing the effective cross sectional area, the pores also lead to local stress concentrations and weaken the material. In the present case it is observed that higher Al_2O_3 contents in the composites tend to offset the deleterious effect of porosity.

4.2.2 Mechanical properties of hydrogen charged material:

The results of the tensile tests conducted on hydrogen pre-charged base and composite specimens are shown in Table 3. Generally, hydrogen charging deteriorates the mechanical properties. In all the cases, the ductility of hydrogen charged specimens were lower than that of uncharged specimens. UTS also decreases with hydrogen charging. The loss in ductility (which is a measure of the degree of hydrogen embrittlement) is maximum for the base material. It is drastically reduced for 2% Al_2O_3 composite and thereupon increases with Al_2O_3 reinforcement fraction. The losses in ductility for the composites on hydrogen charging are however lower than that for the base material. The results obtained can be interpreted by considering the structure and hydrogen trapping behavior of the materials under study.

The properties of the base material, which are inherently poor because of the cast structure, deteriorates the maximum on hydrogen charging when compared to the composites. Microporosities and other casting defects are also present in it. It is a commonly recognized and accepted feature of all previous theories of hydrogen embrittlement that some critical concentration of

hydrogen must be reached at potential crack sites for failure to initiate [8,9]. Hydrogen diffusing through a metal lattice accumulates at metallurgical inhomogeneities/traps [10] and the hydrogen trapping behavior determine the susceptibility to hydrogen embrittlement. Traps for hydrogen may be reversible or irreversible, depending on whether the trapped hydrogen is easily released or tightly bound to the trap. In case the diffusing hydrogen is bound to irreversible traps, it subsequently will not be available for causing embrittlement. However, if hydrogen is reversibly trapped in the material, it is still available for causing embrittlement. In fact, it has been hypothesized that creation of irreversible hydrogen traps should lower materials' susceptibility to hydrogen embrittlement [10]. The different kinds of hydrogen traps present in the materials under study and their hydrogen trapping nature are compared in Table 4.

The base material contains defects in the form of pores that are essentialy reversible hydrogen traps. These reversible traps provide hydrogen for embrittlement. New interfaces are created (i.e,between reinforcement and the matrix) when Al_2O_3 particulates are added to the base material. These incoherent metal-metal oxide interfaces act as irreversible hydrogen traps [10]. Irreversible hydrogen at these interfaces reduces the amount of hydrogen available at potential flaw sites thereby increasing the resistance of composites to hydrogen embrittlement [10]. It has been previously shown that irreversible hydrogen trapping at oxide metal interfaces in $Cu-Al_2O_3$ [11] and $Ni-ThO_2$ [8] systems reduced

Table 4: Type and nature of hydrogen traps in the $Al-Al_2O_3$ composite

Microstructural Feature	Nature of the trap	Variation with increasing Al_2O_3 content
Pores	Reversible	Increases
Grain boundaries	Reversible	Increases
Oxide-Metal Interfaces	Irreversible	Increases

hydrogen embrittlement. Similarly, the addition of TiC, UC, NbC, MO_2C, or TiN to steel reduced the degree of hydrogen embrittlement due to irreversible hydrogen trapping at the interface between these particles and the matrix [9]. In the present case the lower ductility losses on hydrogen charging in the composites compared to the base reflects the positive role of the $Al-Al_2O_3$ interfaces in irreversibly trapping hydrogen. The observed variation of ductility losses with increasing Al_2O_3 volume fractions, however, is due to the interplay between hydrogen trapping at the reversible and irreversible traps. As Al_2O_3 volume fraction increases, the number of irreversible traps also increase because of increasing interfacial area between the matrix and the reinforcement. On the other hand, the grain size decreases with Al_2O_3 volume fraction since these particles act as matrix nucleation sites during the casting of the composites. This increases the effective grain boundary area with increasing Al_2O_3 volume fraction which are reversible traps for hydrogen. Moreover, the porosity content also increases with Al_2O_3 volume fraction. Grain boundaries and pores are reversible hydrogen traps [10]. Therefore, the concentration of both reversible and irreversible traps in $Al-Al_2O_3$ composites increases with increasing volume fraction of Al_2O_3. It appears that the effect of these traps in hydrogen embrittlement phenomenon depends on the Al_2O_3 volume fraction. For example, irreversible hydrogen trapping tends to dominate reversible trapping behavior in $Al-2\%$ Al_2O_3 composite and consequently the ductility loss is the least for this composite.

In the case of Al-4% Al_2O_3 and Al-8% Al_2O_3 composites reversible traps also play a significant role in enhancing hydrogen embrittlement in addition to that played by the irreversible traps (i.e.,metal/oxide interfaces) in lowering hydrogen embrittlement. This is reflected in higher ductility losses upon hydrogen charging for higher volume fractions of Al_2O_3.

Attempts were further made to assess the positive effect of irreversible hydrogen trapping leading to a drastic reduction of hydrogen embrittlement in Al-2% Al_2O_3 composite by repeating the hydrogen pre-charging tests on this material. The results of these duplicate tests are shown in Figure 20. In fact, ductility increased after hydrogen charging in two specimens tested. They showed elongations of 10.08% and 13.15% after hydrogen charging, whereas uncharged Al-2% Al_2O_3 exhibited consistent elongation of only 8.24%. The reason of enhancement of ductility is not clear.

4.3 Results of Corrosion Study:

The results of the polarization studies conducted in 0.1N Hcl on the base and composite materials are presented in Table 5. The corrosion rate given by corrosion current, I_{corr} is found to increase with increasing volume fraction of Al_2O_3 in the particulate composites. The variation of free corrosion potential (FCP) with time is shown in Figure 21. The stabilized FCP, E_{corr} does not bear any systematic relationship with the volume fraction of reinforcement. Figure 21 shows that the FCP of all the materials in 0.1N HCl initially increases with immersion time;
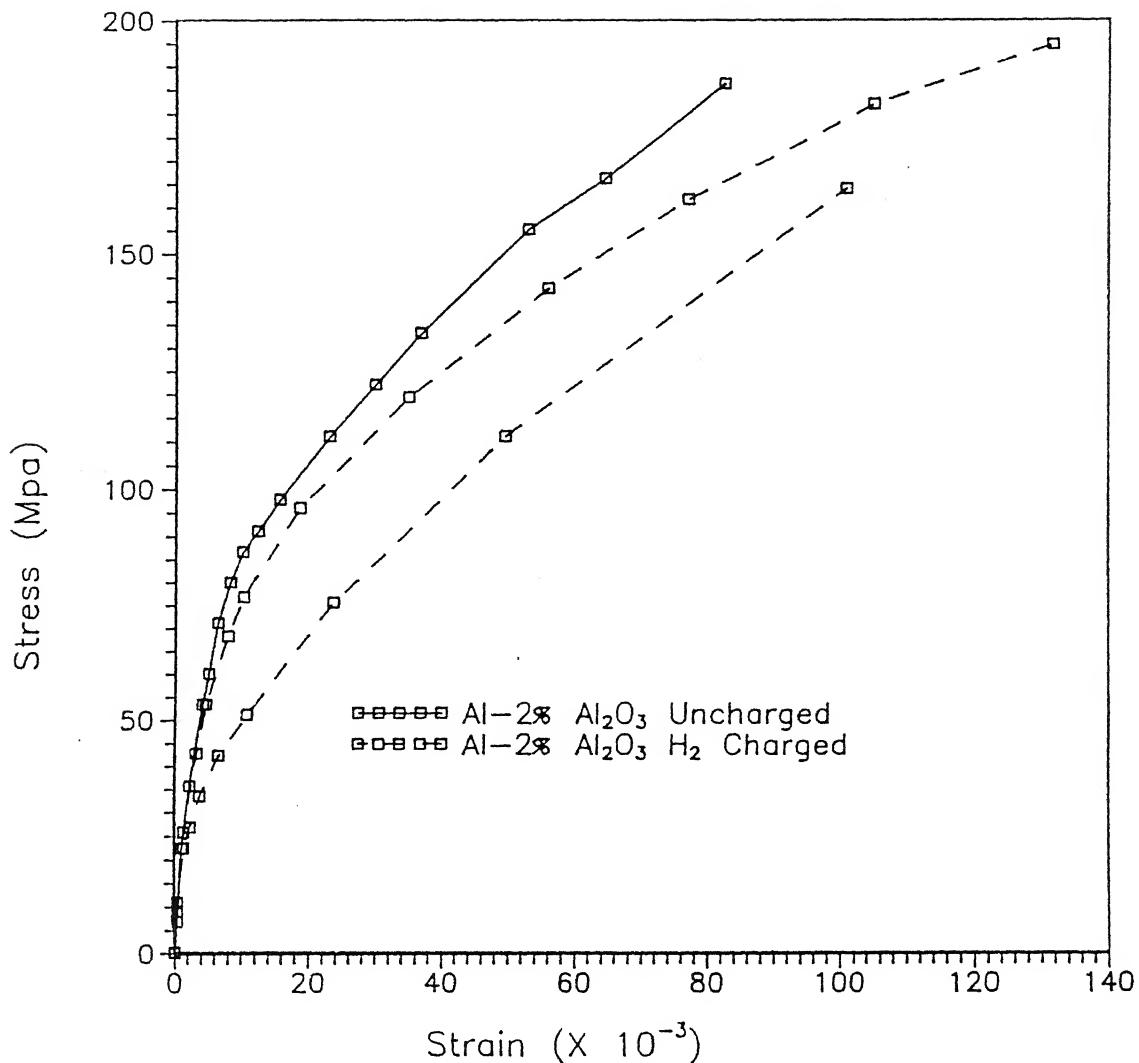
Figure 20.   Engineering stress-strain curves of Al-2% Al$_2$O$_3$ composites
with and without Hydrogen charging (Duplicate tests)

Table 5: Corrosion data obtained from polarization curves.

| Material	E_{corr} (mV Vs SCE)	I_{corr} ($\mu A/cm^2$)
Base	−786	300
Al−2% Al_2O_3	−777	345
Al−4% Al_2O_3	−812	360
Al−8% Al_2O_3	−798	400
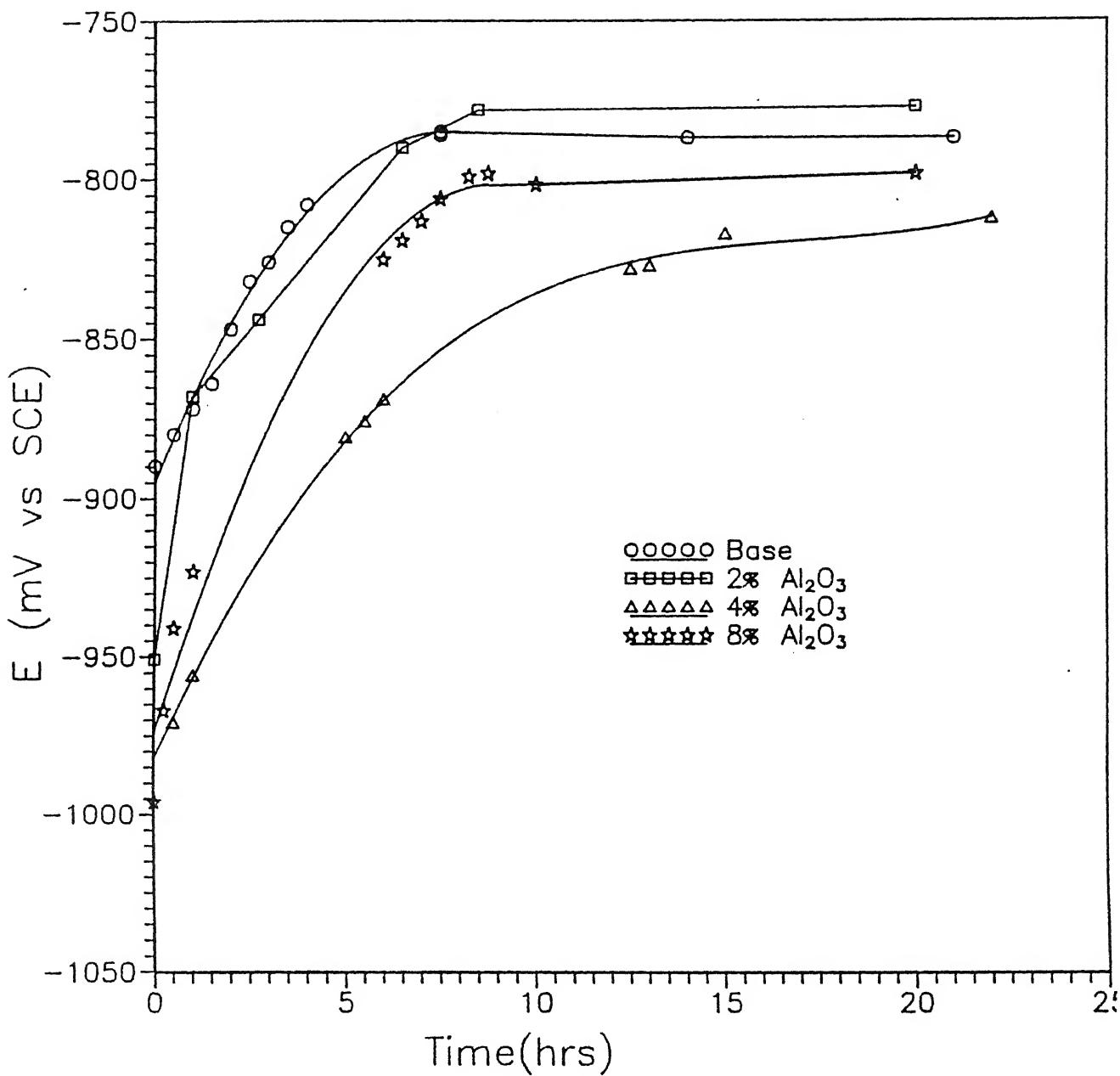
Figure 21.   Variation of free corrosion potential with time in 0.1N HCl

i.e., it becomes noble with increasing time. This time dependence of FCP is attributable to the protective nature of oxide film which forms on the surface on exposure to the aqueous environment. The dispersed reinforcing phase disrupts the formation of a continuous passive film on composites [11,12,13]. This discontinuous oxide film results in an active corrosion potential upon immersion in 0.1N HCl. The increase in FCP after immersion in the solution is due to the formation of a protective oxide film on the surface of these materials. The fairly long times taken to reach the stabilized FCP indicates the slow kinetics of the passivation process. The behavior of FCP with time of these materials is similar to that of pure Al immersed in 1M KCl whose oxide film was totally dissolved in 2N KOH before immersion KCl [15]. Although the E_{corr} values alone cannot provide much information on corrosion rates [16], it does indicate the protective nature of the passive film formed on the surface of the materials on exposure to the corrosive environment.

The stabilized FCP values (Table 5) indicate that the (oxide) film on the composite with 2% Al_2O_3 is most passive and that on the composite with 4% Al_2O_3 is least passive. In order to understand the nature of oxide film covering the surface of these materials, isothermal oxidation studies were conducted in pure oxygen atmosphere at 773K ($500^{o}C$) on all the materials. The oxide film formed on pure aluminium is impermeable to oxygen and the parabolic rate of growth of oxide at high temperatures is governed by the rate of diffusion of Al through the oxide film [17]. In

Al-Mg alloys, Mg rich oxide layers consisting of MgO and $MgAl_2O_4$ form on the surface at high temperatures because the activation energy for Mg diffusion is lower Mg than that of Al in both the metal and the oxide film [17,18]. The results of the oxidation experiments are presented in the weight gain versus time plot (Figure 22). The rate of oxidation as represented by the parabolic rate constant, K_p, is maximum for Al-4% Al_2O_3 and minimum for Al-2% Al_2O_3. This indicates that the oxide layer formed at high temperatures is most protective in the case of Al-2%Al_2O_3 and least protective for Al-4%Al_2O_3. The behavior of the oxide film at high temperatures is similar to that of the passive film that formed upon immersion in 0.1N HCl.

The cathodic polarization curves of the base and composite materials under study are shown in Figure 23. The corrosion rate (I_{corr}) values obtained from these curves (Table 5) indicate that composites corrode faster in 0.1N HCl than the base material. Although Al and its alloys quickly develop a passive film in aqueous media, they are subjected to intense localized corrosion in the presence of "aggressive" anions like chlorides which destabilize the passive film on the surface [15]. In the present case, for the base material, the attack was observed to be relatively uniform. Shrinkage porosities, typical of cast structures, and other casting defects like gas porosities, inclusions and impurities will affect the corrosion rate of the
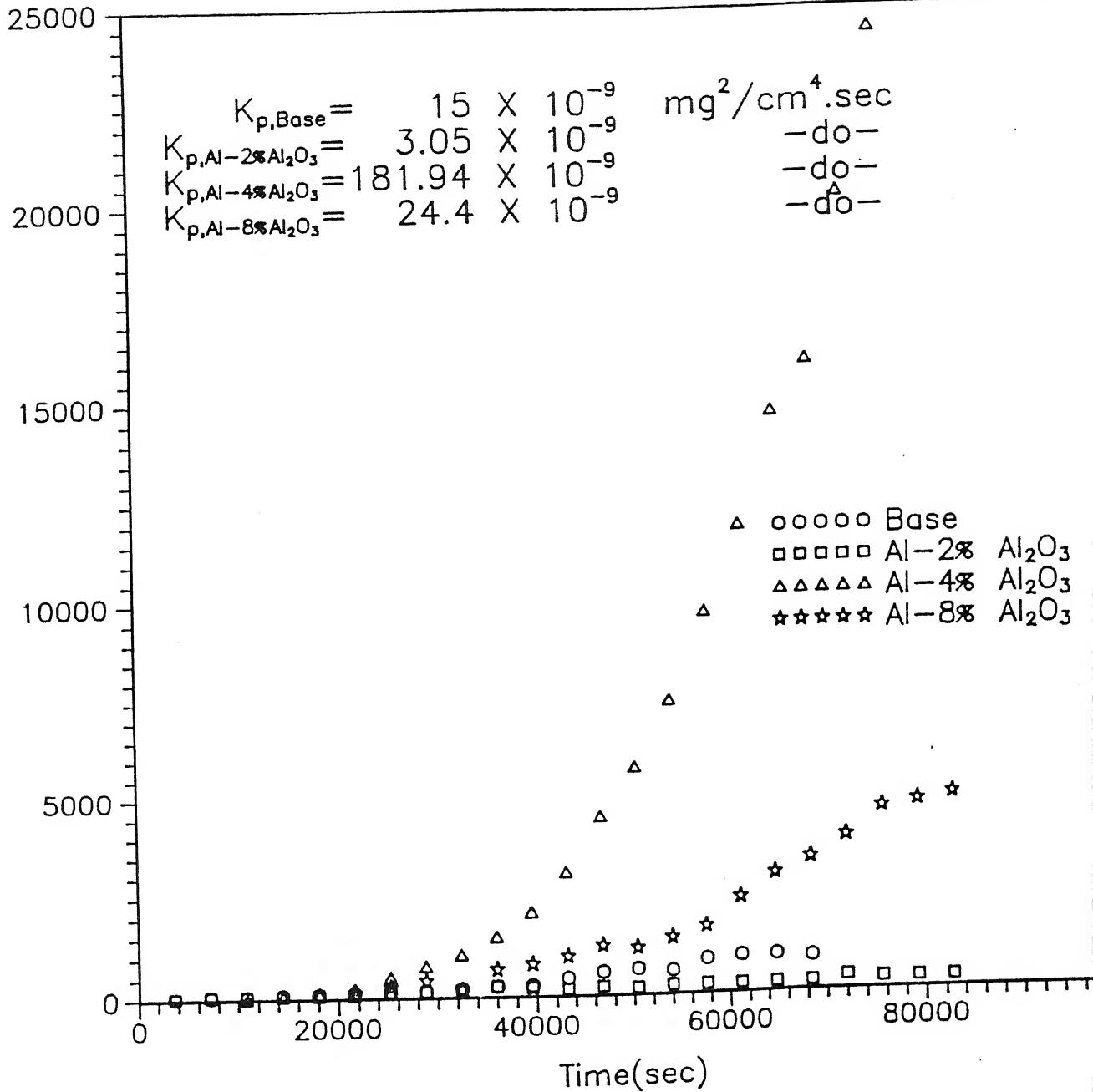
Figure 22. Plot of (Wt gain/Unit area)^2 versus time in oxygen atmosphere at 773K.
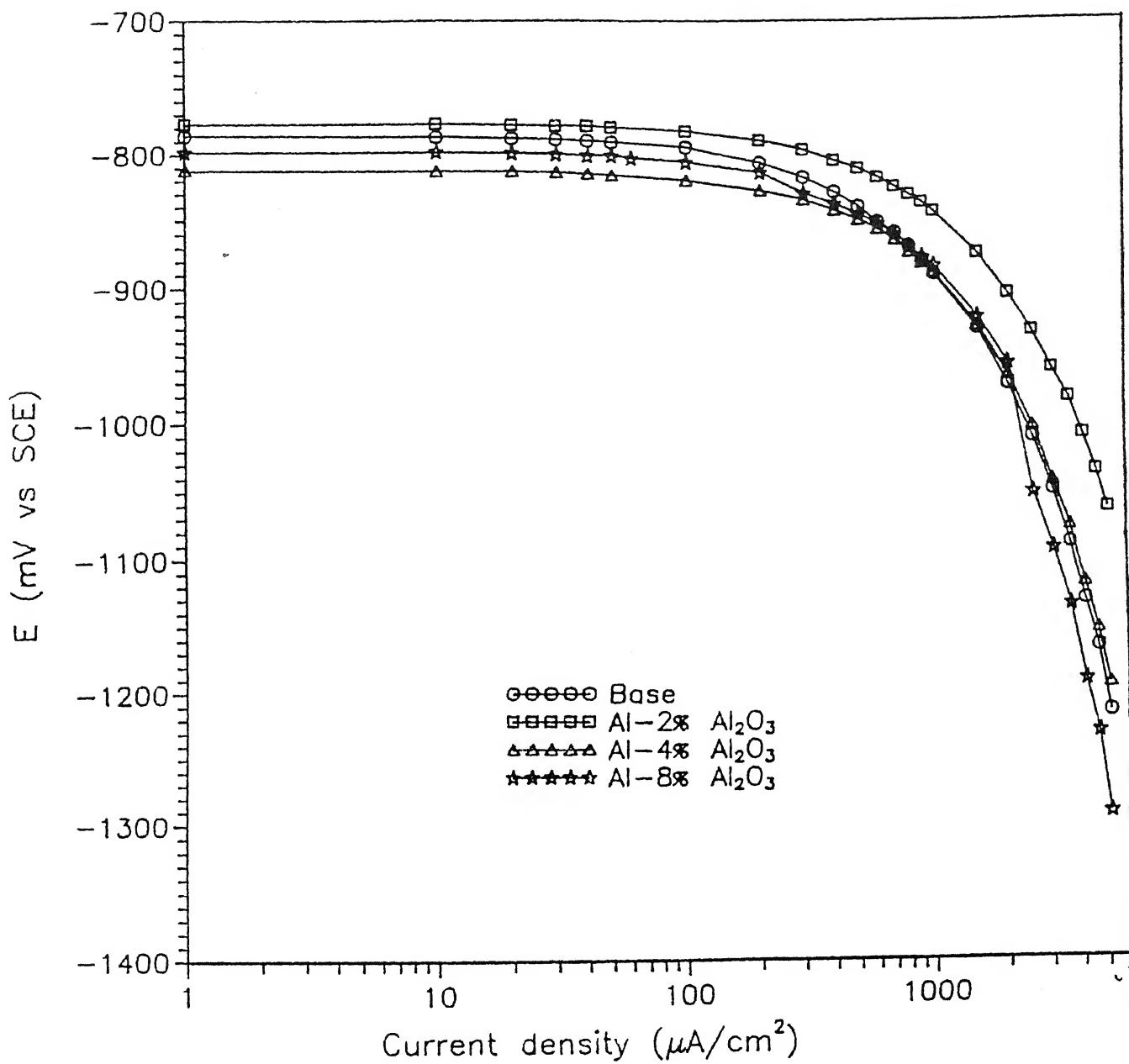
Figure 23. Cathodic polarization curves of base and composite materials in 0.1N HCl.

base material. The increase in porosity content with increasing volume fraction of Al_2O_3 (Figure 15) would also increase the corrosion rate in base as well as the composites. Additionally, in the case of the composites, the particulate-matrix interfaces influences the corrosion rate. The oxide film is not continuous due to the presence of these discontinuities. Therefore corrosion initiates easily at these discontinuities and the composites are susceptible to severe localized corrosion [12,13,14]. Although the extent of localized corrosion may not be reflected in the I_{corr} values determined using Tafel extrapolation studies [13,16], this technique provides information that the corrosion rate increases with increasing volume fraction of reinforcement [12-16,19-22] as observed in the present study.

The potential corrosion initiation sites (i.e., M/MO interfaces) increases with increasing volume fraction of Al_2O_3. and hence corrosion rate also increases with increasing volume fraction of Al_2O_3. It has been previously reported that corrosion rates increase with increasing volume fraction of reinforcement in LM11-SiC [12], 6061-SiC [19], 2014-graphite [20] systems. The deleterious effect of M/MO interfaces on corrosion behavior has also been borne out in the present study.

References:

1. S.Ray, Process Development for Fabrication of Cast Metal Matrix Particulate Composite : Unsolved Problems, Trans.Indian.Inst.Met., 45, 69 (1992).

2. M.V.Ravichandran, R.Krishna Prasad and E.S.Dwarakadasa, Fracture Toughness Evaluation of Aluminium 4% Mg-Al_2O_3 Liquid-Metallurgy Particle Composite, J.Mater.Sci.Let., 11, 452 (1992).

3. P.K.Ghosh, S.Ray and P.K.Rohatgi, Incorporation of Alumina Particles in Aluminium-Magnesium Alloy by Stirring in Melt, Trans. Jap.Inst.Met., 25, 440 (1984).

4. B.C.Pai, Subrata Ray, K.V.Prabhakar and P.K.Rohatgi, Fabrication of Aluminium-Alumina (Magnesia) Particulate Composites in Foundries using Magnesium Additions to the Melts, Matl.Sci.and Eng., 24, 31 (1976).

5. B.F.Quigley, G.J.Abbaschian, R.Wunderlin and R.Mehrabian, A Method for Fabrication of Aluminium-Alumina Composites, Met Trans., 13A, 93 (1982).

6. I.Haginoya and T.Fukusako, Oxidation of molten Al-Mg alloys, Trans Jap Inst Met, 24, 613 (1983).

7. S.Sen, R.Blasubramaniam, and R.Sethuraman, To be published.

8. G.M.Pressouyre, Trap Theory of Hydrogen Embrittlement, Acta Metall., 28, 895 (1980).

9. G.M.Pressouyre and I.M.Bernstein, A Kinetic Trapping Model for Hydrogen-Induced Cracking, Acta Metall., 27, 89 (1979).

10. D.A.Jones,"Principles and Prevention of Corrosion", p336,

Maxwell Macmillan International Publishing Group, New York (1992).

11. Govind, R.Balasubramaniam and G.S.Upadhyaya, Effect of Hydrogen on Ductility of ODS Copper, Scripta Metall., 29, 1303 (1993).

12. O.P.Modi, M.Saxena, B.K.Prasad, A.H.Yagneswaran and M.L.Vaidya, "Corrosion behavior of squeeze-cast aluminium alloy – silicon carbide composites", J.Mater.Sci., 27, 3897 (1992).

13. Deo Nath and T.K.G. Namboodhiri," Some corrosion characteristics of aluminium – mica particulate composites",Corrosion Science, 29, 1215 (1989).

14. H.Sun, E.Y.Koo and H.G.Wheat, " Corrosion behavior of SiC_p/6061 Al Metal Matrix Composites ", Corrosion , 47, 741 (1991).

15. Z.A.Foroulis and M.J.Thubrikar, " On the correspondence between critical pitting potential and pitting of aluminium under conditions of natural immersion ", Electrochemia Acta, 21, 225 (1976).

16. W.H.Ailor," Handbook of corrosion testing and evaluation ", p180-192, John Wiley and Sons, Inc. (1971).

17. C.Lea and J.Ball, " The Oxidation of rolled and heat treated Al-Mg alloys ", Applications of Surface Science, 17, 344 (1984).

18. M.H.Zayana, O.M.Jamjoom and N.A.Razik," High temperature oxidation of Al-Mg alloys ", Oxidation of Metals, 34, 323

(1990).

19. M.S.N.Bhat, M.K.Surappa and H.V.Sudhaker Nayak," Corrosion behavior of silicon carbide particle reinforced 6061/Al alloy composites ", J.Mater.Sci. ,26, 4991 (1991).

20. M.Saxena, B.K.Prasad and T.K.Dan," Corrosion characteristics of aluminium alloy graphite particulate composite in various environment ", J.Mater.Sci., 27, 4805 (1992).

21. D.M.Aylor and P.J.Moran, " Effect of reinforcement on the pitting behavior of Aluminium-base Metal Matrix Composites", J.Electrochem Soc., 132, 1277 (1985).

22. M.Saxena, O.P.Modi, A.H.Yagneswaran and P.K.Rohatgi, " Corrosion characteristics of cast aluminium alloy - 3 Wt% Graphite particulate composites in different environments ", Corrosion Science, 27, 249 (1987).

CONCLUSIONS

1. The $Al-Al_2O_3$ composites prepared by vortex casting exhibited certain extent of particle agglomeration and porosity which are typical of cast microstructures.

2. During the preparation of the composites chemical interaction occurred between the Al_2O_3 particles and Mg to form the reaction product $MgAl_2O_4$. SEM analysis showed that such converted particles were cracked and the cracking is attributed to the stress generated to accommodate the reaction product $MgAl_2O_4$ which occupies a larger volume than does the reactant Al_2O_3.

3. Presence of reacted and cracked Al_2O_3 particles reduced the mechanical properties of the composites. Conversion was maximum in the case of $Al-2\%$ Al_2O_3 composite and this was reflected in mechanical properties. At higher volume fractions extent of conversion decreased and hence the betterment in the mechanical properties.

4. The corrosion rate of Al_2O_3 particulate reinforced Al increased with increasing volume fraction of Al_2O_3 in 0.1N HCl. Presence of reinforcements disrupts the continuity of the oxide film on the surface of the composites and these discontinuities act as potential corrosion initiation sites.

5. The nature of oxide films formed on the surface of these materials during high temperature exposure to oxygen appears to be similar to the nature of the passive films formed on exposure to HCl environment.

6. Hydrogen charging reduced both the ductility and UTS of $Al-Al_2O_3$ composites. The degree of hydrogen embrittlement decreased in composites due to the incorporation of reinforcements. The extent of hydrogen embrittlement is decided by the nature and amount of the hydrogen traps present in the material. At low reinforcement volume fraction, i.e., at 2 weight percentage Al_2O_3, the hydrogen embrittlement is reduced due to the dominant role played by the irreversible traps (i.e.,metal/oxide interfaces). Hydrogen embrittlement increases at higher volume fractions (i.e.,4 and 8 weight percentages) because the dominant role played by the reversible traps offsets the positive effect of irreversible traps.

SUGGESTIONS FOR FURTHER WORK

1. Corrosion and hydrogen embrittlement studies can be carried out on composites with a different reinforcement geometry (platelets or short whiskers) in order to assess the effect of reinforcement geometry on their corrosion and hydrogen embrittlement characteristics.

2. Corrosion studies can be conducted in various other media (containing sulphate or other aggressive ions) also.

3. The drastic reduction of hydrogen embrittlement in $Al-2\%Al_2O_3$ can be further explored.

4. Effect of reinforcement on the high temperature oxidation behavior of composites with regard to the nature of the scale and its growth mechanism can be studied.